RESEARCH ARTICLES

Phosphorylated transcription factor PuHB40 is involved in ROS-dependent anthocyanin biosynthesis in pear exposed to high-light stress

Lu Zhang[1], Lu Wang[1], Yuhao Gao[1], Shulin Yang[1], Jun Su[2], Junbei Ni[1], Yuanwen Teng[1,3] and Songling Bai[1,*]

[1]College of Agriculture and Biotechnology, Zhejiang University, Hangzhou 310058, Zhejiang, China

[2]Institute of Horticulture, Yunnan Academy of Agricultural Sciences, Kunming 650205, China

[3]Hainan Institute of Zhejiang University, Sanya, Hainan 572000, China.

Short title: PuHB40 promotes ROS-dependent anthocyanin biosynthesis

*Corresponding author: Songling Bai (songlingbai@zju.edu.cn)

The author responsible for distribution of materials integral to the findings presented in this article in accordance with the policy described in the Instructions for Authors (https://academic.oup.com/plcell/pages/General-Instructions) is: Songling Bai

(songlingbai@zju.edu.cn).

ABSTRACT

In the context of global warming and climate change, as sessile organisms, plants are more vulnerable to environmental stresses than before. Stress-induced reactive oxygen species (ROS) accumulation results in plant cell damages and even cell death. Anthocyanins are important antioxidants that scavenge ROS to maintain ROS homeostasis. However, the mechanism underlying ROS-induced anthocyanin accumulation is unclear. In this study, we determined that the HD-Zip I family member PuHB40 mediates ROS-dependent anthocyanin biosynthesis under high-light stress. Specifically, PuHB40 is a transcription factor that induces PuMYB123-like/PubHLH3 complex for anthocyanin biosynthesis. The transcriptional activation by PuHB40 depends on its phosphorylation level, which is regulated by protein phosphatase 2A (PP2A). High ROS contents maintain the phosphorylation of PuHB40 at a high level, while also enhancing PuHB40-induced *PuMYB123-like* transcription by decreasing *PuPP2AA2* expression at the transcriptional and translational levels, ultimately leading to increased anthocyanin biosynthesis. Our study revealed the pathway regulating ROS-induced anthocyanin biosynthesis in pear, further clarifying the mechanism underlying abiotic stress-induced anthocyanin biosynthesis, which may have implications for improving plant stress tolerance.

Keywords: high-light stress, ROS, anthocyanin biosynthesis, PuHB40, PuMYB123-like, PP2A phosphatase, dephosphorylation

IN A NUTSHELL

Background: Various abiotic stresses, including high light, promotes the accumulation of anthocyanins in plants. Anthocyanins attenuate the negative effects of on photosynthesis and physiological metabolism of plants under high-light stress by absorbing excess light energy or by acting as an antioxidant to reduce ROS accumulation. Several reports have showed that ROS can stimulate anthocyanin accumulation, but whether the high-light induced anthocyanin accumulation depends on ROS is still under debate. Nevertheless, the underlying mechanism of ROS-dependent anthocyanin biosynthesis is still not clear.

Question: What is the underlying molecular mechanism of high light stress-induced anthocyanin biosynthesis?

Findings: We found that various stresses-induced anthocyanin accumulation in pear plant is dependent on ROS. PuHB40 was the core TF involved in ROS-dependent anthocyanin biosynthesis under high-light stress, while PuMYB13-like is the key MYB TF for anthocyanin biosynthesis in ROS pathway. PuHB40 transcriptionally activates PuMYB123-like/PubHLH3 complex for promoting anthocyanin biosynthesis. The transcriptional activation by PuHB40 depends on its phosphorylation level, which is regulated by protein phosphatase 2A (PP2A). High ROS contents maintain the phosphorylation of PuHB40 at a high level, while also enhancing PuHB40-induced

PuMYB123-like transcription by decreasing *PuPP2AA2* expression at the transcriptional and translational levels, ultimately leading to increased anthocyanin biosynthesis.

Next steps: An important task for next step is to explore whether PuHB40 regulation pathway is applicable in other stresses and provide insight into theoretical basis of abiotic stress-induced anthocyanin biosynthesis. In addition, investigate other post-translational modifications involved in ROS-dependent anthocyanin biosynthesis. Moreover, we will explore the effects of different stress levels on anthocyanin accumulation in pear fruits, and try to regulate pear fruit coloration by appropriate stress.

INTRODUCTION

Because of global warming and climate change, plants are increasingly becoming more susceptible to a variety of environmental stresses (e.g., drought, salinity, cold, and high-light) during growth and development, which leads to changes in physiological and biochemical metabolism, including the dramatic accumulation of reactive oxygen species (ROS) (Hipsch et al. 2021; Mittler et al. 2022). Light is one of the most indispensable environmental factors for plants. It provides energy for photosynthesis to transfer carbon dioxide (CO_2) and water into energy-rich organic matter to sustain plant physiological metabolism (Croce and van Amerongen 2014). Under high-light stress, the flux of photons exceeds the energy that plant need to fix CO_2, O_2^- and $_1O^2$ would primarily produce in the chloroplasts by photosystems i and ii, respectively, and H_2O_2 will also be generated in peroxisomes if photorespiration is activated (Galvez-Valdivieso et al. 2009;

85 Kerchev et al. 2016; Wang et al. 2020; Mittler et al. 2022). Excessive ROS accumulation
86 would disrupt the biological machinery surrounding them, including membranes, proteins
87 and DNA, and then trigger a physiological or programmed pathway for cell death (Lee
88 and Gould 2002; Mittler 2017). Anthocyanins are important secondary metabolites that
89 can function as non-enzymatic antioxidants that maintain ROS homeostasis and limit the
90 damage due to stress-induced ROS. Specifically, anthocyanins decrease ROS production
91 by absorbing light energy at wavelengths that are not readily absorbed by pigments (e.g.,
92 green and blue wavelengths) and limiting the photoinhibitory effects of abiotic stresses
93 (Feild et al. 2001; Hoch et al. 2001; Steyn et al. 2002). They are also antioxidants that
94 serve as ROS scavengers. Notably, their antioxidant capacity is greater than that of other
95 flavonoids or even ascorbic acid and vitamin E (Gould et al. 2002; Bi et al. 2014; Acero
96 et al. 2019). Considering various abiotic stresses promote anthocyanin accumulation in
97 plants (Catala et al. 2011; Xie et al. 2012; Jaakola 2013; Nakabayashi et al. 2014) and
98 ROS can induce anthocyanin production (Xu et al. 2017; Shi et al. 2018), ROS may
99 influence abiotic stress-induced anthocyanin biosynthesis; this hypothesis has been tested
100 in a few studies (Qu et al. 2018).

101 Anthocyanins are synthesized in the phenylpropanoid pathway by various enzymes
102 encoded by structural genes. Examples include phenylalanine ammonia-lyase (PAL),
103 chalcone synthase (CHS), chalcone isomerase (CHI), flavanone 3-hydroxylase (F3H),
104 flavonoid 3′-hydroxylase (F3′H), dihydroflavonol 4-reductase (DFR), anthocyanin

105 synthase (ANS), and UDP-glucose: flavonoid 3-glucosyltransferase (UFGT)
106 (Winkel-Shirley 2001; Koes et al. 2005; Xu et al. 2015). The R2R3-MYB and basic
107 helix–loop–helix (bHLH) transcription factors (TFs) combine with WD-repeat proteins to
108 form MBW complexes in which MYBs function as major regulators of structural gene
109 expression (Koes et al. 2005; Jaakola 2013; Xu et al. 2015). The R2R3-MYB TFs are
110 subdivided into 25 subgroups, among which subgroup 6 contains TFs that are mainly
111 responsible for promoting anthocyanin biosynthesis, including PAP1 (AtMYB75), PAP2
112 (AtMYB90), and AtMYB113 (Dubos et al. 2010). The expression of MYB TFs is
113 regulated by various factors, including light (Takos et al. 2006; Li et al. 2012; Bai et al.
114 2019a), low/high temperatures (Choi et al. 2009; Lin-Wang et al. 2011; Xie et al. 2012),
115 and phytohormones (Shan et al. 2009; Das et al. 2012; Ni et al. 2023). The encoded MYB
116 TFs control the expression of anthocyanin biosynthetic structural genes. To date, the
117 molecular basis of ROS-induced anthocyanin biosynthesis remains relatively
118 uncharacterized.

119 ROS accumulation in cells has an effect on redox state and the post-translational
120 modification of proteins, especially on protein phosphorylation. ROS signal is transduced
121 by Ca^{2+}, Ca^{2+} binding protein, phosphatidic acid (PA) and phospholipase D (PLD) and
122 activates OXIDATIVE SIGNAL-INDUCIBLE 1 (OXI1), which subsequently activates
123 MAPK cascade pathway, which in turn promotes the phosphorylation of downstream
124 transcription factors, such as WRKY proteins and AP2/ethylene-response factors (ERFs)

125 (Kovtun et al. 2000; Jalmi and Sinha 2015; Byrne et al. 2020; Mittler et al. 2022).
126 Furthermore, the phosphorylation of transcription factors are also regulated by
127 phosphatase, such as PTP1, SAL1 and PP2C, whose activity are regulated by ROS levels
128 (Gupta and Luan 2003), oxidative stresses (Chan et al. 2016) or phytohormones (Mine et
129 al. 2017). The PP2A holoenzyme, which is a serine/threonine-specific phosphatase, is a
130 heterotrimeric complex comprising a catalytic subunit C, a regulatory subunit B, and a
131 structural subunit A. The A subunit has a conserved structure consisting of 15 tandem
132 repeats of a 39 amino acid sequence (i.e., HEAT motif) (Janssens and Goris 2001). In *A.*
133 *thaliana*, three A subunits of PP2A have been identified, namely PP2AA1 (RCN1),
134 PP2AA2, and PP2AA3. The phosphatase activity of PP2A plays an important role in
135 stress response (DeLong 2006; Uhrig et al. 2013; Lillo et al. 2014; Durian et al. 2016).
136 However, it is not clear whether PP2A phosphatases are involved in ROS regulation of
137 protein phosphorylation under stress conditions.

138 In this study, we determined that abiotic stress-induced anthocyanin biosynthesis is
139 at least partially dependent on ROS in pear. The HD-Zip I family member PuHB40 was
140 identified as the key TF involved in ROS-dependent anthocyanin biosynthesis. Notably,
141 PuHB40 functions as the upstream positive regulator of the PuMYB123-like/PubHLH3
142 complex during anthocyanin biosynthesis. The dephosphorylation of PuHB40, which is
143 catalyzed by protein phosphatase 2A (PP2A), inhibits its function related to ROS-induced
144 anthocyanin biosynthesis. Under abiotic stress conditions, ROS inhibit the transcription

and translation of *PuPP2AA2*. This study revealed the pathway regulating ROS-induced anthocyanin biosynthesis in pear under high-light stress, providing important insights into the mechanism mediating abiotic stress-induced anthocyanin production.

RESULTS

Stress induced ROS promoted anthocyanin biosynthesis in pear seedling

To test whether abiotic stress-induced anthocyanin biosynthesis depends on ROS production, pear seedlings (*P. ussuriensis*) grown under continuous light were exposed to abiotic stresses, including salt, drought, and high-light, and the ROS scavenger N,N′-dimethylthiourea (DMTU) was used to decrease the ROS content under abiotic stress conditions. The various abiotic stresses caused anthocyanins to accumulate in pear seedlings after 7 days, but anthocyanin production decreased significantly following the DMTU treatment (Supplemental Fig. S1A), indicating that ROS are potentially involved in stress-induced anthocyanin production. Furthermore, ROS accumulation and anthocyanin biosynthesis were examined at 0, 6, 12, 24, 48, 72, and 96 h after plants underwent the high-light stress treatment (Fig. 1A). Anthocyanin accumulation peaked at the 48-h time-point and then decreased, but this accumulation was significantly suppressed in the seedlings that were also treated with DMTU (Fig. 1B). The NBT staining results indicated that the superoxide radical (O^{2-}) accumulated in leaves only after the 6-h time-point, but the accumulation was significantly inhibited by DMTU (Fig. 1C). The DAB staining and quantitative analysis revealed that the accumulation of

165 hydrogen peroxide (H_2O_2) peaked at 48 h and then decreased, but the DMTU treatment
166 suppressed this accumulation (Fig. 1, D and E). Moreover, in response to the different
167 stress treatments (e.g. high-light stress, drought stress, and salt stress), the anthocyanin
168 and H_2O_2 contents increased in the same leaf regions (Supplemental Fig. S1B).
169 According to these results, abiotic stress-induced anthocyanin accumulation depends on
170 ROS production. Hence, the ROS scavenger DMTU can inhibit ROS accumulation and
171 indirectly decrease anthocyanin production.

172 To identify the key genes responsible for abiotic stress-induced anthocyanin
173 biosynthesis, the expression of anthocyanin-related structural and regulatory genes was
174 analyzed. The *PuCHI*, *PuCHS*, *PuDFR*, *PuF3H*, and *PuANS* expression levels increased
175 significantly and peaked at 48 h after the high-light stress treatment, which was in
176 accordance with the changes in anthocyanin accumulation. The expression of these genes
177 was significantly inhibited by DMTU (Fig. 1, F-J). In addition, high-light responsive
178 genes *PuELIP1* and *PuELIP2* were significantly up-regulated in high-light stress
179 treatment and high-light stress plus DMTU treatment compared with the control group,
180 indicating that both groups suffered from high-light stress (Supplemental Fig. S1, C and
181 D). Interestingly, *PuMYB10*, which encodes a critical TF that regulates light-induced
182 anthocyanin biosynthesis in pears, was similarly expressed following the high-light stress
183 and DMTU treatments (Fig. 1K), even though these two treatments resulted in significant
184 differences in anthocyanin accumulation and the expression of downstream structural

genes. These findings suggest that other factors influencing transcription may be involved in regulating ROS-dependent anthocyanin biosynthesis.

Identification of PuMYB123-like and its interaction with PubHLH3

To determine which TFs participate in ROS-dependent anthocyanin biosynthesis, the high-light stress-treated pear seedlings underwent an RNA-seq analysis. Since MYBs TFs play an important role in anthocyanin biosynthesis, we first screened for TFs from the MYB family with expression patterns consistent with anthocyanin biosynthesis structural genes. Finally, we identified a MYB transcription factor, *PuMYB123-like*, whose expression increased rapidly in response to high-light stress and peaked at 48 h, but the DMTU treatment had inhibitory effects on *PuMYB123-like* expression (Fig. 2A). A phylogenetic analysis indicated that *PuMYB123-like* is a homolog of AT5G35550 (AtMYB123) in subgroup 5 (Supplemental Fig. S2A). Moreover, *PuMYB123-like* is most closely related to *MdMYB6* from apple (*Malus domestica*) and *FaMYB9* from strawberry (*Fragaria* × *ananassa*), which are reportedly involved in anthocyanin and proanthocyanidin biosynthesis, respectively (Schaart et al. 2012; Xu et al. 2020) (Fig. 2B). The multiple sequence alignment showed PuMYB123-like contains a typical R2R3 repeat in the N-terminal, with a bHLH motif in the R3 repeat region that can interact with bHLH TFs (Supplemental Fig. S2B). The subcellular localization analysis showed that the fluorescence of GFP-tagged PuMYB123-like was predominantly distributed in the nucleus, consistent with the characteristics of TFs (Fig. 2C). The results of the

205 trans-activation assay suggested PuMYB123-like is a transcriptional activator (Fig. 2D).
206 Considered together, these results indicate that PuMYB123-like is a transcriptional
207 activator that may contribute to ROS-dependent anthocyanin biosynthesis.

208 Considering MYB TFs, bHLHs, and WD-repeat proteins combine to form MBW
209 complexes that control the expression of anthocyanin-related structural genes, we
210 assessed whether PuMYB123-like can interact with three candidate bHLH TFs
211 (PubHLH3, PubHLH33, and PubHLH64). According to the yeast two-hybrid (Y2H)
212 assay results, PuMYB123-like can bind to PubHLH3 (Fig. 2E). The interaction was
213 confirmed in pull-down and luciferase complementation imaging (LCI) assays, which
214 revealed PuMYB123-like can interact with PubHLH3 both *in vivo* and *in vitro* (Fig. 2, F
215 and G). Because of the self-activation of PubHLH33 and PubHLH64, the corresponding
216 genes were fragmented to assess potential interactions. The results showed that
217 PuMYB123-like can interact with the truncated PubHLH64 (encoded by 747–1,086 bp)
218 (Supplemental Fig. S3A), and weakly interact with the truncated PubHLH33 (encoded by
219 588–1,326 bp) (Supplemental Fig. S3B). The dual-luciferase assay demonstrated that
220 PuMYB123-like can significantly activate the promoters of the anthocyanin-related
221 structural genes *PuCHS*, *PuANS*, *PuDFR*, and *PuUFGT* (Fig. 2H). Moreover, PubHLH3
222 significantly enhanced the activation of the *PuCHS* and *PuANS* promoters by
223 PuMYB123-like, but PubHLH33 and PubHLH64 had no significant effect (Fig. 2I and
224 Supplemental Fig. S3C). On the basis of these observations, we speculated that

PuMYB123-like, which belongs to subgroup 2 of the R2R3-MYB family, promotes anthocyanin-related structural genes expression as a component of the MBW complex that includes PubHLH3.

PuMYB123-like promotes anthocyanin biosynthesis in pears

To confirm PuMYB123-like affects anthocyanin biosynthesis, *PuMYB123-like* was overexpressed in pear calli. After a 3-day exposure to light, the anthocyanin contents and anthocyanin-related structural gene expression levels were significantly higher in the calli overexpressing *PuMYB123-like* than in the wild-type calli. In addition, the silencing of *PuMYB123-like* in pear calli via RNA interference (RNAi) inhibited anthocyanin biosynthesis and decreased the expression of anthocyanin-related structural genes (Fig. 3A-C). Considering PuMYB123-like belongs to subgroup 2 of the R2R3-MYB family, which reportedly regulates proanthocyanin biosynthesis, the proanthocyanin content in *PuMYB123-like*-overexpressing (*PuMYB123-like*-OE) pear calli was also examined. There was no significant difference in the proanthocyanin contents of the wild-type and transgenic pear calli (Supplemental Fig. S4A). Additionally, *PuMYB123-like* was ectopically expressed in *Arabidopsis thaliana* to verify the function of the encoded TF. Compared with the wild-type control, the two independent transgenic lines accumulated more anthocyanin (Fig. 3D-F) and had shorter hypocotyls (Fig. 3G). The expression of the anthocyanin-related structural genes *AtCHS*, *AtCHI*, *AtDFR*, *AtF3H*, *AtLODX*, and *AtPAP1* increased significantly in the *PuMYB123-like*-expressing lines (Fig. 3H). To

examine whether PuMYB123-like mediates anthocyanin biosynthesis in fruits, *PuMYB123-like* was transiently overexpressed in the peel of 'Zaosu' pear fruits that were bagged in advance. The comparison with the control peels (empty vector) after a 3-day exposure to light indicated the *PuMYB123-like*-OE peels had significantly higher anthocyanin contents (Supplemental Fig. S4, B and C), and anthocyanin-related structural gene expression levels (i.e., *PpCHS*, *PpDFR*, *PpF3H*, *PpANS*, *PpUFGT*, *PpMYB10*, and *PpMYB114*) (Supplemental Fig. S4D). Similarly, 'Hongzaosu' red pear fruit peels in which *PuMYB123-like* was transiently silenced via virus-induced gene silencing (VIGS) had lower anthocyanin contents and related structural gene expression levels than the control peels (TRV) (Supplemental Fig. S4, E-G). Taken together, these results demonstrate that PuMYB123-like positively regulate the ROS-dependent anthocyanin biosynthesis in pears.

Identification of PuHB40 and its response to ROS

To further investigate the upstream regulator of *PuMYB123-like* in pear, the cis-elements in its promoter were analyzed. Four CAATNATTG motifs (i.e., the binding site of HD-Zip proteins) were identified (Fig. 4A). After screening for HD-Zip-encoding genes with expression patterns similar to that of *PuMYB123-like*, *PuHB40* was identified as a candidate gene. In response to the high-light stress treatment, the *PuHB40* expression level gradually increased after 24 h, peaked at 48 h, and then decreased, but the DMTU treatment significantly inhibited *PuHB40* expression (Fig. 4B). Additionally, the PuHB40

265 content changes in response to ROS were analyzed in an immunoblot involving an
266 affinity-purified anti-PuHB40 polyclonal antibody generated in this study (Supplemental
267 Fig. S5A). The immunoblot results showed that the PuHB40 protein content increased
268 significantly after 6 h of the high-light stress treatment, after which it gradually decreased,
269 but was maintained at a relatively high level. In contrast, the PuHB40 protein level
270 remained low after the DMTU treatment (Fig. 4C). Hence, PuHB40 was affected by ROS
271 at both the transcriptional and translational levels after the abiotic stress treatment.
272 Interestingly, the response of PuHB40 was much faster at the translational level than at
273 the transcriptional level in pear seedlings. To explore whether PuHB40 is responsive to
274 ROS directly, we treated pear calli with 4 mM H_2O_2, which resulted in significantly
275 increased anthocyanin biosynthesis (Fig. 4, D and E). Moreover, the expression of
276 *PcHB40* as well as the anthocyanin-structural genes *PcCHI*, *PcDFR*, *PcF3H*, and *PcANS*
277 also increased (Fig. 4F). Following the H_2O_2 treatment, the *PcHB40* expression level
278 increased after 3 h (Fig. 4G), suggestive of a direct response to H_2O_2.

279 A phylogenetic analysis showed that PuHB40 is a homolog of AT4G36740.1
280 (ATHB40), while a multiple sequence alignment revealed a conserved homeodomain and
281 leucine zipper in PuHB40 (Supplemental Fig. S6, A and B). The trans-activation assay
282 confirmed that PuHB40-BD is a transcriptional activator (Fig. 4H). The subcellular
283 localization analysis detected PuHB40 in the nucleus (Fig. 4I). Accordingly, PuHB40 is a
284 transcriptional activator localized in the nucleus.

PuHB40 promotes *PuMYB123-like* transcript level

On the basis of the presence of four possible PuHB40-binding sites in the *PuMYB123-like* promoter (binding sites 1–4), we hypothesized that PuHB40 may modulate *PuMYB123-like* expression by binding to its promoter. To test this hypothesis, we replaced the possible binding sites with TTTTTTTTT. The dual-luciferase assay detected a significant decrease in the activation of the *PuMYB123-like* promoter by PuHB40 when binding site 4 was mutated (Fig. 5A). The electrophoretic mobility shift assay (EMSA) showed that PuHB40 can directly bind to the *PuMYB123-like* promoter fragment containing binding site 4 (Fig. 5B). The chromatin immunoprecipitation (ChIP) assay revealed the specific enrichment of PuHB40 in the *PuMYB123-like* promoter region harboring binding site 4 (Fig. 5C). Thus, the binding of PuHB40 to site 4 may activate *PuMYB123-like* expression.

To further verify the relationship between PuHB40 and *PuMYB123-like* expression, we transiently overexpressed *PuHB40* and silenced *PuMYB123-like* in pear seedlings. After a 3-day light treatment, anthocyanin accumulation was significantly greater in the *PuHB40*-OE seedlings than in the control seedlings, but the positive effect of PuHB40 on anthocyanin accumulation was significantly inhibited if *PuMYB123-like* was silenced (Fig. 5, D and E); a similar trend was detected in the expression of anthocyanin-related structural genes (Fig. 5F). These results confirmed that PuHB40 promotes anthocyanin biosynthesis in pear by regulating *PuMYB123-like* expression.

PuHB40 positively regulates anthocyanin biosynthesis

To analyze the PuHB40 function related to anthocyanin biosynthesis in pear, *PuHB40*-overexpressing (*PuHB40*-OE) transgenic pear calli and *PuHB40*-RNAi pear calli were generated. After a 2-day exposure to white light, the anthocyanin content was higher in the *PuHB40*-OE transgenic pear calli than in the control calli. Furthermore, anthocyanin accumulation was barely detectable in the *PuHB40*-RNAi pear calli (Fig. 6A-C). A qPCR analysis indicated that the anthocyanin-related genes *PcPAL*, *PcCHI*, *PcDFR*, *PcF3H*, *PcANS*, *PcUFGT*, *PcMYB10* and *PcMYB123-like* were highly expressed in the *PuHB40*-OE pear calli, whereas they were expressed at low levels in the *PuHB40*-RNAi pear calli (Fig. 6D). In addition, *PuHB40* was ectopically expressed in *A. thaliana*. Compared with the wild-type control, three independent transgenic lines ectopically overexpressing *PuHB40* had higher anthocyanin contents (Fig. 6E-G) and shorter hypocotyls (Fig. 6H). Moreover, the ectopic expression of *PuHB40* significantly increased the expression of anthocyanin-related structural genes (Fig. 6I).

To further analyze the *PuHB40* function in pear fruits, bagged mature ‘Zaosu’ and ‘Hongzaosu’ pear fruits were used for transient overexpression and VIGS experiments, respectively. The transient overexpression of *PuHB40* significantly promoted anthocyanin biosynthesis in the pear peel (Supplemental Fig. S7, A and B), while also significantly increasing the expression of anthocyanin-related structural genes and *PpMYB123-like* (Supplemental Fig. S7C). However, compared with the control fruit peel,

the *PuHB40*-TRV fruit peel had a lower anthocyanin content (Supplemental Fig. S7, D and E) and lower anthocyanin-related structural gene and *PpMYB123-like* expression levels (Supplemental Fig. S7F). Accordingly, PuHB40 may be involved in promoting anthocyanin biosynthesis. Considered together, these results imply PuHB40 functions as a positive transcriptional regulator governing anthocyanin production in pear.

Identification of PuPP2AA2 and its interaction with PuHB40

Because the increase in PuHB40 protein abundance occurred much earlier than the increase in the *PuHB40* transcript level, we analyzed the possible post-translational modifications of PuHB40. The PuHB40-interacting proteins in pear seedlings were identified via a GST pull-down assay followed by a mass spectrometry analysis. Among the 36 identified proteins, we focused on the A subunit of PP2A (Supplemental Table S4). According to a phylogenetic analysis, the PP2A A subunit analyzed in the current study is most closely related to the A2 subunit of PP2A in *A. thaliana.* Thus, it was named PuPP2AA2 (Fig. 7A). During the subcellular localization analysis, PuPP2AA2 was detected in the nucleus and cytoplasm (Fig. 7B). The *PuPP2AA2* expression level was significantly lower after the high-light stress treatment than after the DMTU treatment (Fig. 7C). To investigate the response of PuPP2AA2 to ROS at the translational level, we transiently overexpressed the fusion construct encoding MYC-tagged PuPP2AA2 (PuPP2AA2-MYC) in pear seedlings and then exposed the plants to high-light stress conditions with or without a DMTU treatment. The PuPP2AA2 protein abundance

decreased sharply under high-light conditions, but the decrease was significantly attenuated after the DMTU treatment, which presumably decreased the ROS level (Fig. 7D). Thus, PuPP2AA2 is inhibited by high-light stress-induced ROS at both the transcriptional and translational levels.

The GST pull-down assay showed that PuHB40 can interact with PuPP2AA2 *in vitro* (Fig. 7E), whereas the LCI and bimolecular fluorescence complementation (BiFC) assays reflected the interaction between PuHB40 and PuPP2AA2 *in vivo* (Fig. 7, F and G). Taken together, these data confirmed that PuHB40 interacts with the A2 subunit of PP2A, PuPP2AA2, *in vitro* and *in vivo*.

PuPP2AA2 inhibits PuHB40 trans-activation to *PuMYB123-like* by dephosphorylating

To clarify whether the interaction between PuPP2AA2 and PuHB40 affects the phosphorylation status of PuHB40, we transiently overexpressed the fusion construct encoding GFP-tagged PuHB40 (PuHB40-GFP) in *Nicotiana benthamiana* leaves, which were treated with cantharidin (i.e., a widely used PP2A inhibitor) (Honkanen 1993; Ren et al. 2022). We also extracted proteins from the *N. benthamiana* leaves and separated them in a Phos-tag gel and detected the fusion protein using an anti-GFP antibody. One of the two bands detected in the gel corresponded to the phosphorylated form (P+) of PuHB40-GFP, which migrated more slowly than the non-phosphorylated form (P−) of PuHB40-GFP. Moreover, the P+:P− ratio increased after the cantharidin treatment (Fig.

365 8A), indicating that the phosphorylation level increased after PP2A activity was inhibited.
366 To further investigate whether PP2A can directly dephosphorylate PuHB40, we purified
367 the MYC, PuHB40-GFP, and PP2A complex from pear seedlings that were transiently
368 overexpressing the constructs encoding MYC, PuPP2AA2-MYC, and PuHB40-GFP
369 using MYC-Trap and GFP-Trap agarose beads. Because PuPP2AA2 is a structural
370 subunit that is tightly associated with the B and C subunits of the PP2A holoenzyme,
371 other PP2A subunits may be co-purified in the PuPP2AA2-MYC immunoprecipitation
372 complex (Zhou et al. 2004; Ren et al. 2022). Thus, the PP2A complex co-purified by
373 PuPP2AA2-MYC may contain all of the subunits and have phosphatase activity (Ren et
374 al. 2022). We incubated PuHB40-GFP with the MYC and PP2A complex, after which
375 different PuHB40-GFP isoforms were detected using the anti-PuHB40 antibody for the
376 Phos-tag analysis. The incubation with the PP2A complex led to the dephosphorylation of
377 PuHB40 and a decrease in the P+:P− ratio from 0.57 to 0.27 (Fig. 8B), implying PP2A
378 can directly dephosphorylate PuHB40. To confirm that the phosphatase activity of PP2A
379 was responsible for the decrease in the phosphorylation of PuHB40, we deleted the last
380 two tandem repeats (i.e., 14 and 15) of the HEAT motif in the C-terminal of PuPP2AA2.
381 The mutated sequence, which was named PuPP2AA2D, was unable to bind to the B and
382 C subunits of PP2A, thereby preventing the formation of a functional holoenzyme
383 (Ruediger et al. 1994). The subcellular localization analysis showed that PuPP2AA2D
384 was distributed in the nucleus as well as the cytoplasm, similar to the distribution of

385 PuPP2AA2 (Fig. 8C). The LCI and BiFC assays demonstrated that the deletion of tandem
386 repeats 14 and 15 did not affect the interaction between PuPP2AA2D and PuHB40 (Fig.
387 8, D and E).

388 We transiently coexpressed the fusion constructs encoding PuHB40-GFP and
389 PuPP2AA2-MYC as well as the fusion constructs encoding PuHB40-GFP and
390 MYC-tagged PuPP2AA2D (PuPP2AA2D-MYC) in *N. benthamiana* leaves. Different
391 isoforms of PuHB40-GFP were detected by the Phos-tag analysis involving the anti-GFP
392 antibody. Furthermore, the extent of the phosphorylation of PuHB40 decreased
393 significantly after the overexpression of *PuPP2AA2* (i.e., significant decrease in the
394 P+:P− ratio from 6.20 to 1.68), but there was no significant change in the
395 phosphorylation of PuHB40 after the overexpression of *PuPP2AA2D* (i.e.,
396 non-significant decrease in the P+:P− ratio from 6.20 to 5.83) (Fig. 8F). These results
397 indicate PP2A can dephosphorylate PuHB40 *in planta*. Hence, PP2A can
398 dephosphorylate PuHB40 *in vivo* and *in vitro*. Finally, to determine whether PuHB40
399 activity is influenced by its phosphorylation status, the PuHB40-induced transcription of
400 *PuMYB123-like* was determined in a dual-luciferase assay. The presence of PuPP2AA2
401 abolished the ability of PuHB40 to activate *PuMYB123-like* transcription. However, the
402 lack of PP2A phosphatase activity had no significant effect on PuHB40-activated
403 *PuMYB123-like* transcription (Fig. 8G). Therefore, PuHB40 may interact with
404 PuPP2AA2, with the resulting dephosphorylation by PP2A affecting whether PuHB40

can activate the transcription of *PuMYB123-like*.

PP2A attenuates PuHB40-induced anthocyanin biosynthesis

To elucidate the contribution of PuPP2AA2 to anthocyanin biosynthesis in pear, we generated two *PuPP2AA2*-overexpressing transgenic pear calli lines (*PuPP2AA*2-OE #5 and #8), which were subsequently exposed to strong white light for 3 days. The anthocyanin contents were much lower in *PuPP2AA2*-OE #5 and #8 than in the wild-type pear calli (Fig. 9, A and B). The qPCR analysis indicated that the overexpression of *PuPP2AA2* downregulated the expression of anthocyanin-related genes (Fig. 9C). We also transiently silenced and overexpressed *PuPP2AA2* in pear fruit peels. At the injection site of the *PuPP2AA2*-OE fruit peels, there was almost a complete lack of red coloration and the anthocyanin content was lower than that in the control fruit peels (Supplemental Fig. S8, A and B). Moreover, the expression levels of anthocyanin-related genes were significantly lower in the *PuPP2AA2*-OE pear fruit peels than in the control fruit peels (Supplemental Fig. S8C). In contrast, the transient silencing of *PuPP2AA2* significantly promoted anthocyanin accumulation (Supplemental Fig. S8, D and E) and increased the expression of the related structural genes (Supplemental Fig. S8F) suggestive of the negative regulatory effects of PuPP2AA2 on anthocyanin biosynthesis and the red coloration of pear fruits.

To assess whether the phosphorylation status of PuHB40 affects its function associated with ROS-induced anthocyanin biosynthesis in pear, we transiently

425 overexpressed *PuHB40* alone as well as with *PuPP2AA2* in pear seedlings, which were
426 then subjected to a 2-day light treatment. Anthocyanin accumulation and the expression
427 of anthocyanin-related genes as well as *PuMYB123-like* were greater in the pear seedlings
428 overexpressing *PuHB40* alone than in the control seedlings. In contrast, there were no
429 obvious differences in anthocyanin accumulation and the expression of the related genes
430 between the control pear seedlings and the seedlings coexpressing *PuHB40* and
431 *PuPP2AA2* (Fig. 9, D-F). Additionally, bagged mature 'Hongzaosu' pear fruits were used
432 for the transient overexpression of *PuHB40* alone and with *PuPP2AA2*. Compared with
433 the corresponding control levels, the anthocyanin contents and the expression levels of
434 anthocyanin-related genes increased significantly in the pear fruit peels overexpressing
435 *PuHB40* alone, but the presence of PuPP2AA2 weakened the effects of PuHB40 on
436 anthocyanin biosynthesis and the expression of the related genes (Fig. 9, G-I). Thus, the
437 dephosphorylation of PuHB40 by PP2A adversely affects anthocyanin biosynthesis.

438 **DISCUSSION**

439 Plants growing under natural conditions over long periods are increasingly becoming
440 more susceptible to different stresses because of the variability in environmental
441 conditions due to global warming and climate change (Lesk et al. 2016). In plant cells,
442 stress can induce the rapid accumulation of ROS, which are important signaling
443 molecules that activate plant mechanisms related to defense and acclimatization (Mittler
444 et al. 2022). However, excessive amounts of ROS can damage plant cells and may lead to

445 cell death (Mittler 2017) In response to a wide range of stresses and to maintain ROS
446 homeostasis, plants have evolved a series of mechanisms, including those mediating
447 anthocyanin accumulation.

448 In plants, anthocyanins are crucial antioxidants that function as ROS scavengers
449 (Gould et al. 2002; Neill et al. 2002; Bi et al. 2014; Jiang et al. 2023). Many studies
450 showed that anthocyanin accumulation is strongly induced by various stresses, such as
451 high-light stress, ultraviolet radiation, and low temperatures (Steyn et al. 2002; Catala et
452 al. 2011; Xie et al. 2012; Nakabayashi et al. 2014; Landi et al. 2015; Xu et al. 2015). An
453 earlier investigation involving raman spectroscopy confirmed that abiotic stress
454 conditions increase the ROS and anthocyanin contents in the leaves of coleus plants
455 (Altangerel et al. 2017). However, the link between ROS and anthocyanins remains
456 unclear. Although treating *A. thaliana* seedlings with H_2O_2 and ROS activators promotes
457 anthocyanin accumulation (Xu et al. 2017; Shi et al. 2018), evidence of the relationship
458 between ROS and anthocyanin accumulation is lacking. In this study, the ROS scavenger
459 DMTU was applied to eliminate ROS induced by various stresses, thereby serving as a
460 reliable negative control. Stress-induced anthocyanin accumulation in pear seedlings was
461 attenuated by DMTU (Supplemental Fig. S1A), indicating that the increase in the
462 anthocyanin content depends on ROS, which likely function as signaling molecules
463 linking the exposure to different stresses to changes in anthocyanin contents.

464 Anthocyanin biosynthesis is regulated by the MBW complex, with MYB TFs

465 playing a major role and responding to various environmental and internal factors (Xu et
466 al. 2015). R2R3-MYB proteins of subgroup 6 is responsible for anthocyanin biosynthesis
467 (Dubos et al. 2010). In rosaceous plants, MYB10 TFs, which belong to subgroup 6, are
468 essential promotors of light-induced anthocyanin biosynthesis (Takos et al. 2006; Espley
469 et al. 2007; Feng et al. 2010). Although most of the MYB TFs promoting anthocyanin
470 biosynthesis belong to subgroup 6, a few members of other subgroups are also involved.
471 For example, the subgroup 2 members MdMYB9 and MdMYB11 promote jasmonic
472 acid-induced anthocyanin biosynthesis by increasing the expression of
473 anthocyanin-related structural genes (An et al. 2015), whereas MdMYB308L, which is a
474 member of subgroup 4, promotes low-temperature-induced anthocyanin biosynthesis by
475 interacting with MdbHLH33 (An et al. 2020). In the current study, we determined that
476 PuMYB123-like, which belongs to subgroup 2, is the key MYB TF mediating
477 anthocyanin biosynthesis via the ROS-responsive pathway. Traditionally, PuMYB10 has
478 been considered the main MYB TF responsible for anthocyanin biosynthesis in pear
479 (Feng et al. 2010; Bai et al. 2019a), however, its expression is similar following the
480 high-light stress and DMTU treatments (Fig. 1K). The MYB subgroup 2 members are
481 primarily involved in proanthocyanidin biosynthesis, but in the present study, the
482 overexpression of *PuMYB123-like* did not affect proanthocyanidin accumulation in pear
483 calli (Supplemental Fig. S4A). Instead, PuMYB123-like promoted anthocyanin
484 biosynthesis by interacting with PubHLH3 (Fig. 3). Our study findings suggest that

485 members of other MYB subgroups may also have important regulatory effects on
486 anthocyanin biosynthesis, further clarifying the involvement of MYB TFs in
487 ROS-associated anthocyanin biosynthesis.

488 According to earlier research, HD-Zip I family members are crucial regulators of
489 plant responses to stress, especially drought and osmotic stress (Ariel et al. 2007; Harris
490 et al. 2011). But their role in other stresses is less well known. In this study, The HD-Zip I
491 family member PuHB40 was identified as a key TF involved in ROS-regulated
492 anthocyanin biosynthesis under high-light stress (Fig. 4). Considering the important role
493 of HD-Zip I family members in various stresses, PuHB40 regulation pathway for
494 high-light stress-induced anthocyanin biosynthesis might be universal in different stresses.
495 The response of HD-Zip I TFs to drought stress depends on abscisic acid (ABA)
496 (Soderman et al. 1996; Söderman et al. 1999; Olsson et al. 2004), but the relationship
497 with ROS remains unknown. In the current study, PuHB40 responded to high-light stress
498 in an ROS-dependent manner (Fig. 4B), mplying HD-Zip I TFs can respond to other
499 abiotic stresses (i.e., in addition to drought) through multiple signaling pathways. The
500 stability and activity of HD-Zip proteins are regulated by the phosphorylation. In apple,
501 MdHB1 and MdHB2 are phosphorylated by SnRK2 kinase, which enhances their protein
502 stability and activity, thereby activates *MdACO1* expression and promotes ethylene
503 biosynthesis (Jia et al. 2022). In Arabidopsis, ATHB6 is dephosphorylated by the PP2C
504 phosphatase ABI1 by interacting with it directly, thus functions as a negative regulator in

505 the ABA signaling pathway (Himmelbach et al. 2002). The phosphorylation status of
506 HD-Zip I TFs is mainly associated with phytohormone signaling pathway, especially with
507 ABA. In the present study, the phosphorylation of PuHB40 was regulated by ROS via
508 PP2A (Fig. 8). The decrease in the extent of the phosphorylation of PuHB40 decreased
509 the PuHB40-activated transcription of *PuMYB123-like*, ultimately decreasing
510 ROS-induced anthocyanin biosynthesis (Fig. 9, D and G). In plants, PP2A is a ubiquitous
511 and highly conserved serine/threonine-specific phosphatase (Farkas et al. 2007) that
512 catalyzes dephosphorylations with diverse regulatory effects on plant stress responses
513 (Lillo et al. 2014). In general, under salt and osmotic stress conditions, PP2A is inhibited,
514 resulting in phosphorylated target proteins that help protect against various stresses (Bian
515 et al. 2020; Li et al. 2020). However, the effects of ROS on PP2A phosphatase activity
516 under abiotic stress conditions are unclear. In this study, we observed that the structural
517 subunit of PP2A was repressed by ROS at the transcriptional and translational levels in
518 pear (Fig. 7, C and D), suggesting that the regulatory effects of PP2A on plant stress
519 responses may involve ROS. The A subunit of PP2A is the structural subunit that
520 provides a scaffold that binds to the B and C subunits (Kamibayashi et al. 1992; Ruediger
521 et al. 1994; Groves et al. 1999; Janssens and Goris 2001). In *A. thaliana*, three A subunits
522 of PP2A have been identified (RCN1, PP2AA2, and PP2AA3). A mutation to RCN1
523 results in severe phenotypic changes, including stunted growth (dwarfism), abnormal
524 embryogenesis, and sterility. This is in contrast to the mostly normal phenotypes of the

525 *pp2aa2* and *pp2aa3* mutants (Zhou et al. 2004). Thus, it is widely believed that RCN1 is
526 critical for the overall regulation of PP2A, which may help to explain why there have
527 been relatively few studies on PP2AA2 and PP2AA3 (Lillo et al. 2014). In the current
528 study, we revealed that PuPP2AA2 affects ROS-induced anthocyanin biosynthesis by
529 dephosphorylating PuHB40 (Fig. 10), which clarifies the role of the A subunit of PP2A in
530 plants and highlights the importance of the other A subunits.

531 In summary, PuHB40 is the key TF regulating ROS-induced anthocyanin
532 biosynthesis. Specifically, it is a transcriptional activator that induces
533 PuMYB123-like/PubHLH3 complex for anthocyanin biosynthesis. The ability of
534 PuHB40 to activate target gene transcription depends on its phosphorylation level, which
535 is regulated by PP2A. Furthermore, ROS accumulation leads to the extensive
536 phosphorylation of PuHB40 by suppressing PuPP2AA2 production at the transcriptional
537 and translational levels, thereby enhancing the PuHB40-activated transcription of
538 *PuMYB123-like* and promoting anthocyanin biosynthesis (Fig. 10). Our study findings
539 have elucidated the molecular mechanisms by which abiotic stresses regulate anthocyanin
540 biosynthesis in pear, providing insights into how ROS modulate anthocyanin
541 biosynthesis.

542

543 **MATERIALS AND METHODS**

544 **Plant materials and treatment**

Pear seedlings ‘Qingzhen No. 1’ (*Pyrus ussuriensis*: genes from it are prefixed with ‘Pu’) were kindly provided by Professor Wang Ran of Qingdao Agricultural University. The pear seedlings were growth at 25 °C under a 16 h light/ 8 h dark photoperiod (photon flux density 50 $\mu mol \cdot s^{-1} \cdot m^{-2}$). For high-light stress treatment, pear seedlings were exposed to continuous LED white light (photon flux density 160 $\mu mol \cdot s^{-1} \cdot m^{-2}$) in a growth chamber. For salt and drought stress, pear seedlings were growth on solid MS medium supplemented with 30 mM sodium chloride and 2.5% polyethylene Glycol 8000 (PEG 8000) respectively and were exposed to continuous LED white light (photon flux density 50 $\mu mol \cdot s^{-1} \cdot m^{-2}$). For N, N'-dimethylthiourea (DMTU) treatment, seedlings were growth on solid MS medium supplemented with 5 mM DMTU and other condition is same as stress treatment. After treatment, the seedlings were collected, immediately frozen in liquid nitrogen, and stored at -80 °C until used.

Pear calli were generated from the flesh of ‘Clapp’s Favorite’ (*Pyrus communis*: genes from it are prefixed with ‘Pc’) fruitlets as previously described (Bai et al. 2019b). For treatment, the pear calli on good condition were subcultured to the MS solid medium supplemented with 4 mM H_2O_2 for overnight firstly and then were exposed to continuous white light. The pear calli were collected after treatment and stored at -80 °C until used.

Measurement of the total anthocyanin content

The measurement of anthocyanin content is as previously described (Zhang et al. 2022).

Briefly, 0.1 g powder of seedlings, frozen pear calli or peels were soaked in 500 μL methanol: hydrochloric acid (99:1, v/v) solution and incubated overnight at 4 °C in darkness. For pear seedlings, 250 μL chloroform and 250 μL double distilled water were added to the extracting solution for mixing and centrifuged. The supernatant was measured at 530, 657 nm using the DU800 spectrophotometer (Beckman Coulter, Brea, CA, USA).

For pear calli and peels, the extracting solution centrifuged at 4 °C, 12000 rpm, for 10 minutes. And then, the absorbance of supernatant was measured at 530, 620, and 650 nm. The anthocyanin content was calculated as the following formula: $([A_{530}-A_{650}]-0.2\times[A_{650}-A_{620}])/0.1$ for pear calli as well as peels and $(A_{530}-0.25*A_{657})/0.1$ for seedlings.

Histological staining detection of ROS

H_2O_2 and O^{2-} were detected as previously described with minor modification (Xu et al. 2017). Briefly, the leaves of pear seedlings were dipped in DAB staining solution (for H_2O_2 detection) containing 1 mg ml^{-1} DAB and NBT staining solution (for O^{2-} detection) containing 1 mg ml^{-1} NBT. The leaves were incubated for overnight in the dark with gentle shaking (25 °C, 220 rpm min^{-1}). Then, the chlorophyll of leaves was removed with bleaching solution (ethanol: acetic acid: glycerol=3:1:1) by incubating at 85 °C for 30 min. Finally, the leaves were kept in preservative solution (ethanol: glycerol = 4: 1) until images were taken.

586

587 **RNA isolation and reverse transcription quantitative PCR**

588 Total RNA was extracted with a modified CTAB method (Zhang et al. 2012). Genomic
589 DNA removal and first-strand cDNA synthesis from 1 μg RNA were performed with
590 HiScript II First Strand cDNA Synthesis Kit (+gDNA wiper; Vazyme Biotech, China).
591 qPCR was conducted using ChamQ SYBR qPCR Master Mix (Vazyme, China) on CFX
592 Connect real-time PCR system (Bio-Rad, https://www. bio-rad.com/). The relative
593 expression level of genes was calculated using the $2^{-\triangle\triangle Ct}$ method (Livak and Schmittgen
594 2001) with the pear *PpActin* gene (GenBank accession no. JN684184) to normalize the
595 expression values, and the analyses were carried out with three biological replicates. The
596 primers for RT-qPCR are listed in Supplemental Data Set S2.

597

598 **H_2O_2 content quantification**

599 The powder of pear seedlings leaves was soaked in 1 ml of 20 mM potassium phosphate
600 buffer (pH 6.5) on ice and centrifuged, then the supernatant was transferred and
601 additional potassium phosphate buffer was added to 1.5 ml. A 100 μL plant extract was
602 used in each reaction and the H_2O_2 concentration was measured with the Amplex Red
603 hydrogen peroxide/peroxidase assay kit (Thermo Fisher Scientific, Cat. No. A22188).

604

605 **Subcellular localization analysis**

606 Subcellular localization analysis was performed as previously described (Ni et al. 2023).

the full-length complete coding sequences (CDS) (without termination codons) of the target genes (*PuMYB123-like*, *PuHB40*, *PuPP2AA2* and *PuPP2AA2D*) were inserted into pCAMBIA1300 vector to produce *Pro35S: PuMYB123-like-GFP*, *Pro35S: PuHB40-GFP*, *Pro35S: PuPP2AA2-GFP*, and *Pro35S: PuPP2AA2D-GFP*, respectively. *Agrobacterium* strain GV3101 harboring the plasmids were infiltrated into the leaves of *N. benthamiana* transgenic lines containing red fluorescent protein in the nuclei. The GFP and mCherry fluorescence signals were observed by confocal laser scanning microscopy (A1, Nikon, Tokyo, Japan). The primers used for vector construction are listed in Supplemental Data Set S1.

Trans-activation activity assay

A trans-activation activity assay was performed as previously described (Zhang et al. 2022). Briefly, the full-length CDS of *PuMYB123-like* and *PuHB40* was cloned to the pGBKT7 (BD) vector and transformed into yeast *(Saccharomyces cerevisiae)* strain AH109 cells independently. The yeast only containing BD vector is as negative control and yeast containing BD vector with the VP16 fragment (VP16-BD) is as positive control. The yeast transformants were screened on a selective synthetic dextrose medium lacking tryptophan and histidine (SD/-Trp/-His) supplemented with X-α-gal. The primers used for vector construction are listed in Supplemental Data Set S1.

Transient transformation assay in pear fruit and seedlings

628 ‘Hongzaosu’ (also called ‘Red Zaosu’) pear fruits (*Pyrus pyrifolia* × *Pyrus communis*:
629 genes from it are prefixed with ‘Pp’) were collected from the orchard at the Institute of
630 Horticulture, Henan Academy of Agricultural Sciences, Henan, China. Fruits were
631 covered with lightproof double-layered paper bags during the growing season and were
632 harvested about 140 d after full bloom, then immediately transported to the laboratory.
633 Transient transformation assay in pear fruit was performed as previously described (Ni et
634 al. 2023). For the transient overexpression, the full-length CDS of *PuMYB123-like*,
635 *PuHB40* and *PuPP2AA2* was cloned to the pGreenII 0029 62-SK vector and their
636 expression was driven by the 35S promoter. Pear fruits were infiltrated with *A.*
637 *tumefaciens* GV3101 cells containing the plasmid by a needle syringe. For VIGS assay,
638 the gene fragment (~200 to 300 bp) was inserted into the pTRV2 vector (gene-pTRV2)
639 and transformed into *A. tumefaciens* GV3101. Gene-pTRV2 or empty pTRV2 (negative
640 control) was mixed with pTRV1 in equal proportions and co-infiltrated into pear fruits by
641 a needle syringe. After infiltration, pear fruits were exposed to continuous white light (60
642 $\mu mol \cdot m^{-2} \cdot s^{-1}$) and UV-B light (1.1 $\mu mol \cdot m^{-2} \cdot s^{-1}$). The fruit peel surrounding the injection
643 sites was collected and stored at -80 °C until use.

644 For transient transformation assay in pear seedlings, the full-length CDS of *PuHB40*,
645 *PuPP2AA2* and reverse complementary gene fragment (~200 to 300 bp) of
646 *PuMYB123-like* (*PuMYB123-like-RNAi*) were cloned to pCAMBIA1301, and then the
647 plasmids transformed into *A. tumefaciens* GV3101. *A. tumefaciens* GV3101 with

648 *PuHB40* was mixed with pCAMBIA1301, *PuMYB123-like-RNAi*, *PuPP2AA2* in equal
649 proportions and co-infiltrated into seedlings by vacuum (0.8 kg·cm^{-2}, 5 min). The
650 seedlings were then incubated in darkness for 1-2 d and then transferred to a growth
651 chamber for treatment under continuous white light. Finally, the seedlings were collected,
652 frozen in liquid nitrogen immediately, and stored at -80°C until used. The primers used
653 for vector construction are listed in Supplemental Data Set S1.
654
655 **Genetic transformation of pear calli**
656 Transgenic pear calli were generated as previously described (Bai et al. 2019b). Briefly,
657 pear calli were soaked with *A. tumefaciens* EHA105 containing different vectors
658 (PuHB40-pCAMBIA1301, PuMYB123-like-pCAMBIA1301,
659 PuPP2AA2-pCAMBIA1301 for overexpression and PuHB40-RNAi-pCAMBIA1301,
660 PuMYB123-like-RNAi-pCAMBIA1301 for silencing) for 12-15 min and then
661 co-cultured on MS solid medium for 2 d in darkness. Positive pear calli were screened on
662 solid MS medium supplemented with antibiotics (10 mg/L hygromycin B) under
663 continuous darkness at 24 °C for 1-3 months and subcultured every 3 weeks. For light
664 treatment, pear calli in good condition were exposed to continuous white light. The
665 primers used for vector construction are listed in Supplemental Data Set S1.
666
667 **Yeast hybrid assays (Y1H and Y2H)**
668 Yeast one-hybrid assays were performed using the Matchmaker Gold Yeast One-Hybrid

System Kit (TaKaRa) according to the manufacturer's protocol. Briefly, the CDS of *PuHB40* was cloned into the pGADT7 vector, while the promoter fragment of *PuMYB123-like* was ligated into the pAbAi vector. The yeast (*S. cerevisiae*) strain Y1H Gold cells containing both of *PuHB40*-AD and pAbAi-bait were screened on SD/-Leu medium containing an appropriate AbA concentration. The Y2H assay was carried out based with the manufacturer's protocol of Matchmaker Gold Yeast Two-Hybrid System Kit (Takara). The primers used for vector construction are listed in Supplemental Data Set S1.

Pull down screening coupled with LC-MS/MS

The GST-tagged PuHB40 protein (PuHB40-GST) bound to GST-Trap agarose beads were incubated with total proteins of pear seedlings at 4°C for overnight, the GST protein is as negative control. The PuHB40-GST and GST proteins bound to beads were eluted by glutathione (GSH) with gravity column and subjected to immunoblotting analysis with anti-GST antibody. The eluent solution contained PuHB40-GST and GST proteins as well as proteins interacting with PuHB40 in pear seedlings, and then these proteins were further identified by mass spectrometry.

For pull-down assay, His-tagged PuMYB123-like were incubated with GST and GST-tagged PubHLH3 respectively supplemented with GST-Trap agarose beads for overnight, similarly, His-tagged PuHB40 were incubated with GST and GST-tagged PuPP2AA2 respectively. Then they were eluted by GSH and subjected to immunoblotting

analysis with anti-GST antibody and anti-His antibody. The primers used for vector construction are listed in Supplemental Data Set S1.

Luciferase complementation imaging assays

The coding sequences (without termination codons) of PuHB40, PubHLH3 was inserted into pCAMBIA1300-nLUC vectors, and the CDS of PuMYB123-like, PuPP2AA2 and PuPP2AA2D was cloned to pCAMBIA1300-cLUC vectors. The vectors were introduced into *Agrobacterium* strain GV3101 individually and *A. tumefaciens* harboring gene-nLUC were mixed with an equal volume of *Agrobacteria* containing gene-cLUC and then co-infiltrated into *N. benthamiana* leaves. Five minutes before detection, 10 mM beetle luciferin (Promega) was injected into the same position as the agrobacteria and then captured by ChemiDoc™XRS+ (Bio-Rad). The *N. benthamiana* leaves co-infiltrated with empty vectors expressing cLUC and nLUC as a negative control. The primers used for vector construction are listed in Supplemental Data Set S1.

Bimolecular fluorescence complementation assay

The full-length PuHB40 was inserted into p2YC and p2YN, while PuPP2AA2 and PuPP2AA2D were cloned to p2YN and p2YN respectively. Then, *A. tumefaciens* GV3101 cells harboring gene-p2YN and gene-p2YC mixed in equal proportions and co-infiltrated into *N. benthamiana* leaves by injection, Leaves were co-infiltrated with gene-2YN and 2YC or 2YN and 2YC-gene as the negative control. The YFP signal was

711 detected by a confocal laser scanning microscope (Nikon, Japan) after 48 h-72 h. The
712 primers used for vector construction are listed in Supplemental Data Set S1.
713
714 **Dual-luciferase assay**
715 Dual-luciferase assays were performed as previously reported (Bai et al. 2019a). The
716 full-length CDS of PuHB40, PuPP2AA2 and PuPP2AA2D were cloned into pGreenII
717 0029 62-SK vector (gene-SK) and the fragments of *PuMYB123-like* promoter were
718 ligated into pGreenII 0800-LUC vector (promoter-LUC). All vectors were transformed
719 into *A. tumefaciens* strain GV3101 cells harboring the pSoup vector. *A. tumefaciens* strain
720 GV3101 contaning gene-SK and promoter-LUC were injected into *N. benthamiana*
721 leaves at a ratio of 1:10. The firefly luciferase and Renilla luciferase activities were
722 analyzed at 48 h after the infiltration by the Dual-Luciferase Reporter Assay System
723 (Promega) and the GloMax96 Microplate Luminometer (Promega). The primers used for
724 vector construction are listed in Supplemental Data Set S1.
725
726 **Electrophoretic mobility shift assay**
727 The 3' end biotin-labeled double-stranded DNA probes were prepared by annealing 3'
728 end biotin-labeled oligonucleotides to the corresponding complementary strands (95 °C
729 for 5 min and 70 °C for 20 min). The EMSA were performed using the Light-Shift^{TM}
730 Chemiluminescent EMSA Kit (Thermo Scientific) based with manufacturer's protocol.

731 Briefly, recombinant PuHB40-His protein was incubated with labeled or nonlabeled
732 double-stranded probes at room temperature for 20 min in binding buffer. The samples
733 were then separated by 6.5% (w/v) native polyacrylamide gels at 4 °C and the
734 biotin-labeled probes was captured with ChemiDoc™XRS+ (Bio-Rad). The
735 oligonucleotide probes used in this study are listed in Supplemental Data Set S1.
736
737 **ChIP assay**
738 The ChIP assays were performed as previously described (Ni et al. 2023). The pear calli
739 transformed with the recombinant PuHB40-MYC construct and the empty construct
740 (MYC alone) were prepared for ChIP assays. The pear calli were treated in 1% (w/v)
741 formaldehyde under vacuum for 10 min for the cross-linking and then the chromatin was
742 extracted via sucrose gradient centrifugation. The chromatin DNA was sonication for 30
743 min on ice (30 s with 30 s intervals) with the Bioruptor Plus device (Diagenode) to shear
744 the chromatin to an average size of 200 bp to 500 bp. The sheared chromatin was
745 incubated with Anti-MYC (Sigma-Aldrich, 05-724) at 4 °C overnight and the amount of
746 immunoprecipitated chromatin was determined by qPCR. Each ChIP assay was repeated
747 3 times, and the enriched DNA fragments in each ChIP sample served as 1 biological
748 replicate for qPCR. The primers used for the ChIP-qPCR analysis are listed in
749 Supplemental Data Set S3.
750

751 **Mn^{2+}-Phos-tag SDS-PAGE**

752 Prior to Phos-tag analysis, samples need to be pretreated by TCA precipitation and then
753 protein samples were detected by 10% regular SDS-PAGE supplemented with 60 μM
754 Phos-tag (TM) Acrylamide AAL-107 (Wako) and 120 μM $MnCl_2$. Wash the gels by
755 gently agitating it 10 minutes for 3 times using general transfer buffer supplemented with
756 10 mmol/L EDTA after electrophoresis for 1.5 h and then washed by general transfer
757 buffer for 10 min. Finally, the gels were used for immunoblotting analysis.

758

759 **Protein dephosphorylation assays *in vitro* and *vivo***

760 For dephosphorylation assays in vitro, *A. tumefaciens* GV3101 with PuHB40-GFP,
761 PuPP2AA2-MYC and MYC infiltrated into pear seedlings by vacuum (0.8 $kg \cdot cm^{-2}$, 5
762 min). Then, PuHB40-GFP, PuPP2AA2-MYC and MYC were purified by
763 immunoprecipitation from pear seedlings with GFP-Trap and MYC-Trap agarose beads.
764 Purified PuPP2AA2-MYC was used as PP2A complex, since other subunits of PP2A
765 could co-immunoprecipitate by PuPP2AA2. Equal volume of purified PuHB40-GFP
766 mixed with PuPP2AA2-MYC and MYC respectively and then incubated an oscillator
767 (1200 g, 30 °C) for 2 h, which was terminated by adding protein loading buffer and
768 boiled at 98 °C for 10 min. Finally, the mixtures were used for immunoblotting analysis.

769 For dephosphorylation assays *in vivo*, *A. tumefaciens* GV3101 with PuHB40-GFP
770 was mixed with MYC, PuPP2AA2-MYC, PuPP2AA2D-MYC in equal proportions and

co-infiltrated into *N. benthamiana* leaves by injection. The total proteins were extracted from *N. benthamiana* leaves after 48 h-72 h and subjected to TCA precipitation, immediately followed by Phos-tag analyses. For cantharidin treatment, *A. tumefaciens* GV3101 with PuHB40-GFP infiltrated into *N. benthamiana* leaves by injection and 50 μM cantharidin was injected into the same position as the agrobacteria after 24 h, and then treated for 24 h. Finally, the total proteins were extracted and then used for Phos-tag analyses.

Statistical analysis

All data in this study were analyzed using two-sided Student's *t*-test or one-way analysis of variance (ANOVA) to determine statistical significance with GraphPad Prism v.9.0. Detailed statistical analysis data are shown in Supplemental Data Set S5.

ACCESSION NUMBERS

Sequence data from this article can be found in an online pear genome database (https://ngdc.cncb.ac.cn/gwh/Assembly/18534/show): PuHB40 (EVM0020592.1), PuMYB123-like (EVM0034726.1), PuPP2AA2 (EVM0003533.1), PubHLH3 (EVM0031731.1), PubHLH33 (EVM0038434.1), PubHLH64 (EVM0003136.1), PuELIP1 (EVM0019834.1), PuELIP2 (EVM0035306.1), PuCHS (EVM0036585.1), PuCHI (EVM0024725.1), PuF3H (EVM0021098.1), PuDFR (EVM0012887.1), PuANS (EVM0001840.1), PuUFGT (EVM0026501.1), PuMYB10 (EVM0039871.1),

PuMYB114 (EVM0020507.1).

SUPPLEMENTAL DATA

Supplemental Figure S1. Stresses induced anthocyanin biosynthesis is ROS-dependent.

Supplemental Figure S2. Identification of PuMYB123-like.

Supplemental Figure S3. The interaction between PuMYB123-like and PubHLHs.

Supplemental Figure S4. Functional analysis of PuMYB123-like in 'Hongzaosu' and 'Zaosu' pear fruit.

Supplemental Figure S5. Detection of specific anti-PuHB40 polyclonal antibody.

Supplemental Figure S6. Identification of PuHB40.

Supplemental Figure S7. Functional analysis of PuHB40 in 'Hongzaosu' and 'Zaosu' pear fruit.

Supplemental Figure S8. Functional analysis of PuPP2AA2 in 'Hongzaosu' pear fruit.

Supplemental Data Set S1. Primers used for constructing vectors or EMSA in this study.

Supplemental Data Set S2. Primers for qPCR analysis in this study.

Supplemental Data Set S3. Primers for ChIP-qPCR analysis in this study.

Supplemental Data Set S4. PuHB40 possible interacting proteins were identified with GST pull-down combined with mass spectrometry.

Supplemental File S1. Protein sequences used to generate phylogenetic tree in Fig. 2B.

Supplemental File S2. Phylogenetic tree of Fig. 2B in Newick format.

Supplemental File S3. Protein sequences used to generate phylogenetic tree in Fig. 7A.

Supplemental File S4. Phylogenetic tree of Fig. 7A in Newick format.

Supplemental File S5. Protein sequences used to generate phylogenetic tree in Fig. S2A.

Supplemental File S6. Phylogenetic tree of Fig. S2A in Newick format.

Supplemental File S7. Protein sequences used to generate phylogenetic tree in Fig. S6A.

Supplemental File S8. Phylogenetic tree of Fig. S6A in Newick format.

ACKNOWLEDGMENTS

We thank R. Wang at Qingdao Agricultural University for providing pear seedlings of 'Qingzhen No. 1' (*Pyrus ussuriensis*). We also thank Kunfeng Li for technical help and providing plant materials.

FUNDING INFORMATION

This work was supported by the Zhejiang Provincial Natural Science Foundation of China under Grant No. LR22C150001, The National Natural Science Foundation of China (32072545 to YT, 32272639 to SB, 32269745 to JS), and the China Agriculture Research System of MOF and MARA.

AUTHOR CONTRIBUTIONS

Y.T and S.B. planned the work. S.B. and L.Z. conceived and designed the experiments.

L.Z. performed most experiments. L.W., S.Y. helped conduct some of the experiments. Y.G. and J.S. helped to analyze the data. L.Z. and S.B wrote the manuscript and, Y.T., J.N. helped to revise the manuscript. All authors read and approved the final paper.

DECLARATION OF INTERESTS

The authors declare that they have no competing interests.

FIGURE LEGENDS

Figure 1. High light stress-induced anthocyanin biosynthesis is ROS-dependent.
A-K), Pear seedlings were treated with high light stress treatment (photon flux density: approximately 160 $\mu mol \cdot s^{-1} \cdot m^{-2}$) or high light stress supplemented with N, N'-dimethylthiourea (DMTU) treatment. DMTU was applied as ROS scavenger, and pear seedlings under appropriate light condition were used as Mock (photon flux density: approximately 50 $\mu mol \cdot s^{-1} \cdot m^{-2}$). Pear seedlings were sampled at 0 h, 6 h, 12 h, 24 h, 48 h, 72 h, 96 h. **A)**, Phenotype of pear seedlings (scale bar, 1 cm). **B)**, The anthocyanin content for pear seedlings. **C and D)**, NBT staining for superoxide and DAB staining for H_2O_2 in pear seedlings leaves, respectively (scale bar, 0.5 mm). **E)**, H_2O_2 quantification of pear seedlings. **F-K)**, The expression levels of *PuCHI*, *PuCHS*, *PuDFR*, *PuF3H*, *PuANS*, *PuMYB10* in pear seedlings under different treatments. *PuACTIN* was amplified as an internal control. Data are presented as means ± s.d. of 3 biological replicates. Asterisks indicate significant differences compared with Mock group (two-tailed Student's *t-test*, $*P < 0.05$, $**P < 0.01$), all exact *P* values are shown in Supplemental Data Set S5.

Figure 2. Identification of PuMYB123-like and its interaction with PubHLH3.
A) The expression levels of *PuMYB123-like* in pear seedlings under high-light stress treatment or high-light stress supplemented with DMTU treatment, and pear seedlings

under appropriate light condition were used as Mock. *PuACTIN* was amplified as an internal control. **B)** Phylogenetic analysis of PuMYB123-like. The phylogenetic tree was generated using the Maximum-likelihood method of MEGA (version 10.1.8). Bootstrap values from 1000 replicates for each branch are shown. The protein sequences from pear (Pu, *Pyrus pyrifolia*, highlighted with blue dots), apple (Md, *Malus* × *domestica*, highlighted with green dots), Arabidopsis (At, *Arabidopsis thaliana*, highlighted with rose red dots) and strawberry (Fa, *Fragaria* × *ananassa*, highlighted with purple dots). PuMYB123-like (EVM0034726.1) is bolded and enlarged. **C)** Subcellular localization of PuMYB123-like in *N. benthamiana* leaf cells (scale bar, 25 μm). **D)** Trans-acting activity of PuMYB123-like in yeast cells. **E)** Interaction between PuMYB123-like and PubHLH3 in a yeast two-hybrid assay, with pGADT7-T and pGBKT7-53 as positive controls. DDO, SD/-Trp/-Leu medium; QDO/X/A, SD/-Trp/-Leu/-Ade/-His medium with X-α-gal and Aureobasidin. **F)** The interaction between PuMYB123-like and PubHLH3 was detected by luciferase complementation imaging assays. The pseudocolour scale bar indicates the range of luminescence intensity. **G)** The interaction between PuMYB123-like and PubHLH3 analyzed using a pull-down assay. PuMYB123-like-His was incubated with GST or PubHLH3-GST. The interaction proteins were precipitated by GST-Trap agarose beads and analysed by immunoblotting with an anti-GST or anti-His antibody. **H)** A dual-luciferase assay demonstrated that PuMYB123-like promotes the promoter activity of anthocyanin-related genes (*PuCHS*, *PuANS*, *PuDFR*, *PuUFGT*). The promoter of anthocyanin-related genes was cloned into the pGreenII 0800-LUC (firefly luciferase) vector, and the full-length CDS of *PuMYB123-like* was cloned into the pGreenII 0029 62-SK vector. The empty vector of pGreenII 0029 62-SK was used as control. **I)** Dual-luciferase assay showed that interaction between PuMYB123-like and PubHLH3 significantly enhanced activation of PuMYB123-like on *PuCHS* and *PuANS* promoters. Data are presented as means ± s.d. of 3 biological replicates **A)** and 6 biological replicates **H)** and **I)**. Asterisks indicate significant differences compared with Mock **A)**, empty vector **H)** and PuMYB123-like **I)** (two-tailed Student's *t-test*, $*P < 0.05$, $**P < 0.01$), all exact *P* values are shown in Supplemental Data Set S5.

Figure 3. PuMYB123-like promotes anthocyanin biosynthesis.

A) Phenotype of pear calli overexpressing and silencing *PuMYB123-like* (scale bar, 1 cm). Wild type pear calli were used as the negative control. Pear calli were incubated under continuous white light at 17°C for 3 d. **B)** Expression levels of anthocyanin-related genes and *PuMYB123-like* in *PuMYB123-like*-OE *and PuMYB123-like*-RNAi pear calli after light treatment. *PcACTIN* was amplified as an internal control. **C)** Anthocyanin contents in *PuMYB123-like*-OE and *PuMYB123-like*-RNAi pear calli after light treatment. **D)** Phenotype of Arabidopsis seedlings overexpressing *PuMYB123-like* (scale bar, 2 mm). Wild-type 'Columbia 0' was used as the negative control. Arabidopsis seedlings were grown on 1/2 MS medium for 5 days. **E)** Expression levels of *PuMYB123-like* in transgenic Arabidopsis lines. *AtPP2A* was amplified as an internal control. **F)** Anthocyanin contents in transgenic Arabidopsis lines. **G)** The hypocotyl length of transgenic Arabidopsis seedlings. **H)** Expression levels of anthocyanin-related genes in transgenic Arabidopsis lines. Data are presented as means ± s.d. of 3 biological replicates **B)**, **C)**, **E)**, **F)** and **H)** and 15 biological replicates **G)**. Asterisks indicate significant differences compared with wild type pear calli **B)** and **C)**, wild type Arabidopsis **E-H)**, (two-tailed Student's *t-test*, $*P < 0.05$, $**P < 0.01$), all exact P values are shown in Supplemental Data Set S5.

Figure 4. Identification of PuHB40 and its response to ROS.

A) Distribution of potential binding sites of PuHB40 in *PuMYB123-like* promoter region. Vertical red lines indicate the position of site1 to site4. **B)** The expression levels of *PuHB40* in pear seedlings under high-light stress treatment or high-light stress supplemented with DMTU treatment, and pear seedlings under appropriate light condition were used as Mock. *PuACTIN* was amplified as an internal control. **C)** Changes in the PuHB40 abundance in pear seedlings under high-light stress treatment or high-light stress supplemented with DMTU treatment for 0 h, 6 h, 24 h, 48 h. The PuHB40 protein was detected by immunoblotting with an affinity-purified specific anti-PuHB40 polyclonal antibody. **D)** Phenotype of pear calli after 4 mM H_2O_2 treatment for 2 days (scale bar, 1 cm). Pear calli treated with 0 mM H_2O_2 were used as control. **E)**

Anthocyanin contents in pear calli treated with 0 mM or 4 mM H_2O_2 for 2 days. **F)** Expression levels of *PcHB40*, *PcMYB123-like* and anthocyanin-related genes in pear calli treated with 0 mM or 4 mM H_2O_2 for 2 days. *PcACTIN* was amplified as an internal control. **G)** Expression levels of *PcHB40* in pear calli after 0 mM or 4 mM H_2O_2 treatment for 0 h, 3 h, 6 h, 12 h, 24 h, 72 h. *PcACTIN* was amplified as an internal control. **H)** Trans-acting activity of PuHB40 in yeast cells. **I)** Subcellular localization of PuHB40 in *N. benthamiana* leaf cells (scale bar, 25 μm). Data are presented as means ± s.d. of 3 biological replicates. Asterisks indicate significant differences compared with Mock **B)**, 4 mM H_2O_2 **E-F)** (two-tailed Student's *t-test*, $*P < 0.05$, $**P < 0.01$), all exact *P* values are shown in Supplemental Data Set S5.

Figure 5. PuHB40 positively regulates anthocyanin biosynthesis by promoting *PuMYB123-like* transcription.

A) Effect of potential binding sites mutation on the activation of *PuMYB123-like* by PuHB40. Four potential binding sites (site1 to site4) were mutated into TTTTTTTTT, respectively. The promoters of *PuMYB123-like* with or without potential binding site mutation were cloned into the pGreenII 0800-LUC (firefly luciferase) vector, and the full-length CDS of *PuHB40* was cloned into the pGreenII 0029 62-SK vector. The empty vector of pGreenII 0029 62-SK was used as control. **B)** An EMSA confirmed that PuHB40 binds directly to the site4 in the *PuMYB123-like* promoter. The *ProPuMYB123-like* probe was the biotin-labeled fragment of *PuMYB123-like* promoter containing site4 (AAATTATTG), whereas the cold probe was an unlabeled probe (50-, 100-, and 200-fold molar excess). *ProPuMYB123-like*-mut probe was the same as the *ProPuMYB123-like* probe but with site4 (AAATTATTG) mutated to TTTTTTTTT. The His-tagged PuHB40 protein was purified. **C)** ChIP-qPCR assay results reflected the in vivo binding of PuHB40 to the *PuMYB123-like* promoter. Cross-linked chromatin samples were extracted from *PuHB40*-MYC-overexpressing pear calli with 3 biological replicates and precipitated with an anti-MYC antibody. Eluted DNA was used to amplify *PuMYB123-like* promoter fragments and eight regions (P1 to P8) were examined, among which P6 containing site4. Pear calli overexpressing the MYC sequence were used as a

negative control. Three biological replicates of pear calli were used in the ChIP assay. **D)** Transient overexpression of *PuHB40* with or without transient silencing of *PuMYB123-like* in pear seedlings. The full-length CDS of *PuHB40* and reverse complementary gene fragment (~200 to 300 bp) of *PuMYB123-like* were inserted into the pCAMBIA1301 vector for the subsequent expression under the control of the 35S promoter. The plasmids were transformed into *A. tumefaciens* GV3101 and infiltrated into pear seedlings by vacuum. The infiltrated pear seedlings were firstly incubated in darkness for 2 days and then exposed to continuous white light for 3 days. Pear seedlings infiltrated with an empty pCAMBIA1301 vector were used as a control. **E)** Anthocyanin content in pear seedlings. **F)** Expression levels of *PuHB40*, *PuMYB123-like* and anthocyanin-related genes in pear seedlings. Data are presented as means ± s.d. of 3 biological replicates **C), E)**, **F)** and 6 biological replicates **A)**. Asterisks indicate significant differences compared with empty vector **A)** and control **C), E)**, **F)** (two-tailed Student's *t-test*, $*P < 0.05$, $**P < 0.01$; ns, no significance, $P > 0.05$), all exact P values are shown in Supplemental Data Set S5.

Figure 6. PuHB40 promotes anthocyanin biosynthesis.

A) Phenotype of pear calli overexpressing and silencing *PuHB40* (scale bar, 1 cm). Wild type pear calli were used as the negative control. Pear calli were incubated under continuous white light at 17°C for 3 d. **B) a**nd **D)** Expression levels of *PuHB40*, *PpMYB123-like* and anthocyanin-related genes in *PuHB40*-OE and *PuHB40*-RNAi pear calli after light treatment. *PcACTIN* was amplified as an internal control. **C)** Anthocyanin contents in *PuHB40*-OE and *PuHB40*-RNAi pear calli after light treatment. **E)** Phenotype of Arabidopsis seedlings overexpressing *PuHB40* (scale bar, 2 mm). Wild-type 'Columbia 0' was used as the negative control. Arabidopsis seedlings were grown on 1/2 MS medium for 5 days. **F)** Expression levels of *PuHB40* in transgenic Arabidopsis lines. *AtPP2A* was amplified as an internal control. **G)** Anthocyanin contents in transgenic Arabidopsis lines. **H)** The hypocotyl length of transgenic Arabidopsis seedlings. **I)** Expression levels of anthocyanin-related genes in transgenic Arabidopsis lines. Data are presented as means ± s.d. of 3 biological replicates **B-D)**, **F), G), I)** and 15 biological

replicates **H)**. Asterisks indicate significant differences compared with wild type pear calli **B-D)** and wild type Arabidopsis **F-I)** (two-tailed Student's *t-test*, $*P < 0.05$, $**P < 0.01$), all exact *P* values are shown in Supplemental Data Set S5.

Figure 7. Identification of PuPP2AA2 and its interaction with PuHB40.

A) Phylogenetic analysis of PuPP2AA2. The phylogenetic tree was generated using the Maximum-likelihood method of MEGA (version 10.1.8). Bootstrap values from 1000 replicates for each branch are shown. The protein sequences from pear (Pu, *Pyrus pyrifolia*, highlighted with blue dots) and Arabidopsis (*Arabidopsis thaliana*, highlighted with rose red dots). PuPP2AA2 (EVM0003533.1) is bolded and enlarged. **B)** Subcellular localization of PuPP2AA2 in *N. benthamiana* leaf cells (scale bar, 25 μm). **C)** The expression levels of *PuPP2AA2* in pear seedlings under high-light stress treatment or high-light stress supplemented with DMTU treatment. *PuACTIN* was amplified as an internal control. **D)** Changes in the PuPP2AA2 abundance in pear seedlings. Pear seedlings transiently overexpressed MYC-tagged *PuPP2AA2* and were exposed to high-light stress treatment or high-light stress supplemented with DMTU treatment for 0 h, 3 h, 6 h, 12 h. The PuPP2AA2 protein was detected by immunoblotting with anti-MYC monoclonal antibody. **E)** The interaction between PuPP2AA2 and PuHB40 using a pull-down assay. PuHB40-His was incubated with GST or PuPP2AA2-GST. The interaction proteins were precipitated by GST-Trap agarose beads and analysed by immunoblotting with an anti-GST or anti-His antibody. **F)** The interaction between PuPP2AA2 and PuHB40 was detected by luciferase complementation imaging assays. The pseudocolour scale bar indicates the range of luminescence intensity. **G)** Physical association between PuPP2AA2 and PuHB40 confirmed by a BiFC assay. Fluorescence indicates positive interactions (scale bar, 25 μm). Data are presented as means ± s.d. of 3 biological replicates. Asterisks indicate significant differences compared with high-light stress supplemented with DMTU treatment (two-tailed Student's *t-test*, $*P < 0.05$), all exact *P* values are shown in Supplemental Data Set S5.

Figure 8. PuHB40 was dephosphorylated by PP2A phosphatase.

A) Phos-tag analysis of phosphorylation of PuHB40 after cantharidin treatment. *A. tumefaciens* GV3101 containing PuHB40-GFP plasmid infiltrated into *N. benthamiana* leaves by injection and 50 μM cantharidin was injected into the same position as the agrobacteria after 24 h. *N. benthamiana* leaves injected corresponding concentration of DMSO were used as negative control. Protein samples were extracted from *N. benthamiana* leaves after 24 h and were separated in a Phos-tag gel (upper panel), and PuHB40-GFP with different phosphorylated status was detected using the anti-GFP antibody. Total PuHB40-GFP proteins were analyzed by SDS-PAGE without Phos-tag (indicated as "Regular"), and were detected using anti-GFP antibody. P+ and P- indicate phosphorylated and non-phosphorylated form of PuHB40, respectively. The intensity of the bands was measured with the Image J software and was calculated as the ratio of the P+/P- form. **B)** Immunoblotting analysis showing that the PP2A complex directly dephosphorylates PuHB40 *in vitro*. MYC, PP2A complex, and PuHB40-GFP were immunopurified from pear seedlings transiently overexpressing MYC, PuPP2AA2-MYC, and PuHB40-GFP using MYC-Trap or GFP-Trap, respectively. After incubation of PP2A complexes with PuHB40-GFP (MYC with PuHB40-GFP was set as control), protein samples in the reaction system were separated in Phos-tag gel (upper panel) and detected using the anti-PuHB40 antibody. The intensity of the bands was measured with the Image J software and calculated as the ratio of the P+/P-. Total proteins in the reaction system were analyzed by SDS-PAGE without Phos-tag (indicated as "Regular"). MYC, PuPP2AA2-MYC, and PuHB40-GFP were set as the loading controls and detected by the anti-MYC or anti-PuHB40 antibody, respectively. **C)** Subcellular localization of PuPP2AA2D in *N. benthamiana* leaf cells (scale bar, 25 μm). PuPP2AA2D is PuPP2AA2 with heat repeats 14 and 15 in the C-terminal deleted. **D)** The interaction between PuPP2AA2D and PuHB40 confirmed by a BiFC assay. Fluorescence indicates positive interactions (scale bar, 25 μm). **E)** The interaction between PuPP2AA2D and PuHB40 was detected by luciferase complementation imaging assays. The pseudocolour scale bar indicates the range of luminescence intensity. **F)** Immunoblotting analysis showing that PP2A dephosphorylates PuHB40 *in vivo*. Protein extracts from *N. benthamiana* leaves

co-infiltrated PuHB40-GFP with MYC, PuPP2AA2-MYC, or PuPP2AA2D-MYC were separated in Phos-tag gel (upper panel) and detected using the anti-GFP antibody (MYC with PuHB40-GFP was set as control). The intensity of the bands was measured with the Image J software and calculated the ratio of P+/P−. Total PuHB40-GFP, MYC, PuPP2AA2-MYC and PuPP2AA2D-MYC proteins were analyzed by SDS-PAGE without Phos-tag (indicated as "Regular"). PuHB40-GFP, MYC, PuPP2AA2-MYC and PuPP2AA2D-MYC were set as the loading controls and detected by the anti-GFP or anti-MYC antibody, respectively. **G)** Dual-luciferase assay showed that dephosphorylation of PuHB40 by PP2A significantly inhibited the activation of *PuMYB123-like* promoter by PuHB40. The *PuMYB123-like* promoter was cloned into the pGreenII 0800-LUC (firefly luciferase) vector, and the full-length CDS of *PuHB40*, PuPP2AA2 and PuPP2AA2D was cloned into the pGreenII 0029 62-SK vector. The PuHB40 was used as control. Data are presented as means ± s.d. of 6 biological replicates **G)**. Asterisks indicate significant differences compared PuHB40 **G)** (two-tailed Student's *t-test*, $^{**}P < 0.01$; ns, no significance, $P > 0.05$), all exact P values are shown in Supplemental Data Set S5.

Figure 9. Attenuation of PuHB40-induced anthocyanin biosynthesis by PuPP2AA2. **A)** Phenotype of pear calli overexpressing *PuPP2AA2* (scale bar, 1 cm). Wild type pear calli were used as the negative control. Pear calli were incubated under continuous white light at 17°C for 3 d. **B)** Anthocyanin contents in *PuPP2AA2*-OE after light treatment. **C)** Expression levels of *PuPP2AA2* and anthocyanin-related genes in *PuPP2AA2*-OE pear calli after light treatment. *PcACTIN* was amplified as an internal control. **D)** Transient overexpression of *PuHB40* with or without transient overexpressing of *PuPP2AA2* in pear seedlings. The full-length CDS of *PuHB40* and *PuPP2AA2* were inserted into the pCAMBIA1301 vector for the subsequent expression under the control of the 35S promoter. The plasmids were transformed into *A. tumefaciens* GV3101 and infiltrated into pear seedlings by vacuum. The infiltrated pear seedlings were firstly incubated in darkness for 2 days and then exposed to continuous white light for 3 days. Pear seedlings infiltrated with an empty pCAMBIA1301 vector were used as a control. **E)** Anthocyanin

content in pear seedlings. **F)** Expression levels of *PuHB40*, *PuPP2AA2*, *PuMYB123-like* and anthocyanin-related genes in pear seedlings. **G)** Transient overexpression of *PuHB40* with or without transient overexpressing of *PuPP2AA2* in fruit (scale bar, 1 cm). The full-length CDS of *PuHB40* and *PuPP2AA2* were cloned to the pGreenII 0029 62-SK vector for the subsequent expression under the control of the 35S promoter. Pear fruits were infiltrated with *A. tumefaciens* GV3101 cells containing the recombinant plasmid using a needle-free syringe. Fruits infiltrated with an empty pGreenII 0029 62-SK vector were used as a control. The phenotypes were examined after a 1 day dark and 4 days light treatment. **H)** Total anthocyanin content in pear fruits. **I)** Expression levels of *PuHB40*, *PuPP2AA2* and anthocyanin-related genes in pear fruits. Data are presented as means ± s.d. of 3 biological replicates. Asterisks indicate significant differences compared with wild type pear calli **B)** and **C)**, empty vector **E), F), H), I)** (two-tailed Student's *t-test*, $*P < 0.05$, $**P < 0.01$; ns, no significance, $P > 0.05$), all exact P values are shown in Supplemental Data Set S5.

Figure 10. Proposed model for PuHB40-mediated ROS-dependent anthocyanin biosynthesis in pears.

PuHB40 is the key transcription factor in ROS-induced anthocyanin biosynthesis. ROS promote PuHB40 expression and then positively regulate its transcriptional activity on PuMYB123-like/PubHLH3 complex to induce anthocyanin biosynthesis. The transcriptional activity of PuHB40 depends on its phosphorylation level which is regulated by PP2A. ROS maintain phosphorylation of PuHB40 at a high level, and enhance the transcriptional activity of PuHB40 on *PuMYB123-like* by reducing the transcriptional and translational levels of PuPP2AA2 under high-light stress, and thus promote anthocyanin biosynthesis. The lightning indicates the intensity of transcriptional regulation of *PuMYB123-like* by PuHB40.

REFERENCES

Acero N, Gradillas A, Beltran M, Garcia A, Munoz Mingarro D. Comparison of

1096 phenolic compounds profile and antioxidant properties of different sweet cherry
1097 (*Prunus avium* L.) varieties. Food Chem. 2019:**279**:260-271.
1098 https://doi.org/10.1016/j.foodchem.2018.12.008

1099 **Altangerel N, Ariunbold GO, Gorman C, Alkahtani MH, Borrego EJ, Bohlmeyer D,**
1100 **Hemmer P, Kolomiets MV, Yuan JS, Scully MO.** In vivo diagnostics of early abiotic
1101 plant stress response via Raman spectroscopy. Proc Natl Acad Sci U S A.
1102 2017:**114**(13):3393-3396. https://doi.org/10.1073/pnas.1701328114

1103 **An JP, Wang XF, Zhang XW, Xu HF, Bi SQ, You CX, Hao YJ.** An apple MYB
1104 transcription factor regulates cold tolerance and anthocyanin accumulation and
1105 undergoes MIEL1-mediated degradation. Plant Biotechnol J. 2020:**18**(2):337-353.
1106 https://doi.org/10.1111/pbi.13201

1107 **An XH, Tian Y, Chen KQ, Liu XJ, Liu DD, Xie XB, Cheng CG, Cong PH, Hao YJ.**
1108 MdMYB9 and MdMYB11 are involved in the regulation of the JA-induced
1109 biosynthesis of anthocyanin and proanthocyanidin in apples. Plant Cell Physiol.
1110 2015:**56**(4):650-662. https://doi.org/10.1093/pcp/pcu205

1111 **Ariel FD, Manavella PA, Dezar CA, Chan RL.** The true story of the HD-Zip family.
1112 Trends Plant Sci. 2007:**12**(9):419-426. https://doi.org/10.1016/j.tplants.2007.08.003

1113 **Bai S, Tao R, Yin L, Ni J, Yang Q, Yan X, Yang F, Guo X, Li H, Teng Y.** Two B-box
1114 proteins, PpBBX18 and PpBBX21, antagonistically regulate anthocyanin biosynthesis
1115 via competitive association with *Pyrus pyrifolia* ELONGATED HYPOCOTYL 5 in the

peel of pear fruit. Plant J. 2019a:**100**(6):1208-1223. https://doi.org/10.1111/tpj.14510

Bai S, Tao R, Tang Y, Yin L, Ma Y, Ni J, Yan X, Yang Q, Wu Z, Zeng Y, et al. BBX16, a B-box protein, positively regulates light-induced anthocyanin accumulation by activating *MYB10* in red pear. Plant Biotechnol J. 2019b:**17**(10):1985-1997. https://doi.org/10.1111/pbi.13114

Bi X, Zhang J, Chen C, Zhang D, Li P, Ma F. Anthocyanin contributes more to hydrogen peroxide scavenging than other phenolics in apple peel. Food Chem. 2014:**152**:205-209. https://doi.org/10.1016/j.foodchem.2013.11.088

Bian C, Guo X, Zhang Y, Wang L, Xu T, DeLong A, Dong J. Protein phosphatase 2A promotes stomatal development by stabilizing SPEECHLESS in *Arabidopsis*. Proc Natl Acad Sci U S A. 2020:**117**(23):13127-13137. https://doi.org/10.1073/pnas.1912075117

Byrne DP, Shrestha S, Galler M, Cao M, Daly LA, Campbell AE, Eyers CE, Veal EA, Kannan N, Eyers PA. Aurora A regulation by reversible cysteine oxidation reveals evolutionarily conserved redox control of Ser/Thr protein kinase activity. Sci Signal. 2020:**13**(613). https://doi.org/10.1126/scisignal.aax2713

Catala R, Medina J, Salinas J. Integration of low temperature and light signaling during cold acclimation response in *Arabidopsis*. Proc Natl Acad Sci U S A. 2011:**108**(39):16475-16480. https://doi.org/10.1073/pnas.1107161108

Chan KX, Mabbitt PD, Phua SY, Mueller JW, Nisar N, Gigolashvili T, Stroeher E,

Grassl J, Arlt W, Estavillo GM, et al. Sensing and signaling of oxidative stress in chloroplasts by inactivation of the SAL1 phosphoadenosine phosphatase. Proc Natl Acad Sci U S A. 2016:**113**(31):E4567-4576. https://doi.org/10.1073/pnas.1604936113

Choi S, Kwon YR, Hossain MA, Hong S-W, Lee B-h, Lee H. A mutation in *ELA1*, an age-dependent negative regulator of *PAP1/MYB75*, causes UV- and cold stress-tolerance in *Arabidopsis thaliana* seedlings. Plant Sci. 2009:**176**(5):678-686. https://doi.org/10.1016/j.plantsci.2009.02.010

Croce R, van Amerongen H. Natural strategies for photosynthetic light harvesting. Nat Chem Biol. 2014:**10**(7):492-501. https://doi.org/10.1038/nchembio.1555

Das PK, Shin DH, Choi SB, Yoo SD, Choi G, Park YI. Cytokinins enhance sugar-induced anthocyanin biosynthesis in Arabidopsis. Mol Cells. 2012:**34**(1):93-101. https://doi.org/10.1007/s10059-012-0114-2

DeLong A. Switching the flip: protein phosphatase roles in signaling pathways. Curr Opin Plant Biol. 2006:**9**(5):470-477. https://doi.org/10.1016/j.pbi.2006.07.015

Dubos C, Stracke R, Grotewold E, Weisshaar B, Martin C, Lepiniec L. MYB transcription factors in *Arabidopsis*. Trends Plant Sci. 2010:**15**(10):573-581. https://doi.org/10.1016/j.tplants.2010.06.005

Durian G, Rahikainen M, Alegre S, Brosche M, Kangasjarvi S. Protein Phosphatase 2A in the Regulatory Network Underlying Biotic Stress Resistance in Plants. Front Plant Sci. 2016:**7**:812. https://doi.org/10.3389/fpls.2016.00812

Espley RV, Hellens RP, Putterill J, Stevenson DE, Kutty-Amma S, Allan AC. Red colouration in apple fruit is due to the activity of the MYB transcription factor, MdMYB10. Plant J. 2007:**49**(3):414-427. https://doi.org/10.1111/j.1365-313X.2006.02964.x

Farkas I, Dombradi V, Miskei M, Szabados L, Koncz C. *Arabidopsis* PPP family of serine/threonine phosphatases. Trends Plant Sci. 2007:**12**(4):169-176. https://doi.org/10.1016/j.tplants.2007.03.003

Feild TS, Lee DW, Holbrook NM. Why Leaves Turn Red in Autumn. The Role of Anthocyanins in Senescing Leaves of Red-Osier Dogwood. Plant Physiol. 2001:**127**(2):566-574. https://doi.org/10.1104/pp.010063

Feng S, Wang Y, Yang S, Xu Y, Chen X. Anthocyanin biosynthesis in pears is regulated by a R2R3-MYB transcription factor PyMYB10. Planta. 2010:**232**(1):245-255. https://doi.org/10.1007/s00425-010-1170-5

Galvez-Valdivieso G, Fryer MJ, Lawson T, Slattery K, Truman W, Smirnoff N, Asami T, Davies WJ, Jones AM, Baker NR, et al. The high light response in *Arabidopsis* involves ABA signaling between vascular and bundle sheath cells. Plant Cell. 2009:**21**(7):2143-2162. https://doi.org/10.1105/tpc.108.061507

Gould KS, McKelvie J, Markham KR. Do anthocyanins function as antioxidants in leaves? Imaging of H_2O_2 in red and green leaves after mechanical injury. Plant Cell Environ. 2002:**25**(10):1261-1269. https://doi.org/10.1046/j.1365-3040.2002.00905.x

Groves MR, Hanlon N, Turowski P, Hemmings BA, Barford D. The structure of the protein phosphatase 2A PR65/A subunit reveals the conformation of its 15 tandemly repeated HEAT motifs. Cell. 1999:**96**(1):99-110. https://doi.org/10.1016/S0092-8674(00)80963-0

Gupta R, Luan S. Redox control of protein tyrosine phosphatases and mitogen-activated protein kinases in plants. Plant Physiol. 2003:**132**(3):1149-1152. https://doi.org/10.1104/pp.103.020792

Harris JC, Hrmova M, Lopato S, Langridge P. Modulation of plant growth by HD-Zip class I and II transcription factors in response to environmental stimuli. New Phytol. 2011:**190**(4):823-837. https://doi.org/10.1111/j.1469-8137.2011.03733.x

Himmelbach A, Hoffmann T, Leube M, Hohener B, Grill E. Homeodomain protein ATHB6 is a target of the protein phosphatase ABI1 and regulates hormone responses in *Arabidopsis*. Embo J. 2002:**21**(12):3029-3038. https://doi.org/10.1093/emboj/cdf316

Hipsch M, Lampl N, Zelinger E, Barda O, Waiger D, Rosenwasser S. Sensing stress responses in potato with whole-plant redox imaging. Plant Physiol. 2021:**187**(2):618-631. https://doi.org/10.1093/plphys/kiab159

Hoch WA, Zeldin EL, McCown BH. Physiological significance of anthocyanins during autumnal leaf senescence. Tree Physiol. 2001:**21**(1):1-8. https://doi.org/10.1093/treephys/21.1.1

Honkanen RE. Cantharidin, another natural toxin that inhibits the activity of

1196 serine/threonine protein phosphatases types 1 and 2A. FEBS Lett.
1197 1993:**330**(3):283-286. https://doi.org/10.1016/0014-5793(93)80889-3
1198 **Jaakola L.** New insights into the regulation of anthocyanin biosynthesis in fruits. Trends
1199 Plant Sci. 2013:**18**(9):477-483. https://doi.org/10.1016/j.tplants.2013.06.003
1200 **Jalmi SK, Sinha AK.** ROS mediated MAPK signaling in abiotic and biotic stress-
1201 striking similarities and differences. Front Plant Sci. 2015:**6**:769.
1202 https://doi.org/10.3389/fpls.2015.00769
1203 **Janssens V, Goris J.** Protein phosphatase 2A: a highly regulated family of
1204 serine/threonine phosphatases implicated in cell growth and signalling. Biochem J.
1205 2001:**353**(3):417-439. https://doi.org/10.1042/0264-6021:3530417
1206 **Jia M, Li X, Wang W, Li T, Dai Z, Chen Y, Zhang K, Zhu H, Mao W, Feng Q, et al.**
1207 SnRK2 subfamily I protein kinases regulate ethylene biosynthesis by phosphorylating
1208 HB transcription factors to induce *ACO1* expression in apple. New Phytol.
1209 2022:**234**(4):1262-1277. https://doi.org/10.1111/nph.18040
1210 **Jiang T, He Y, Wu Z, Cui Y, Wang X, Huang H, Fan Y, Han M, Wang J, Wang S, et**
1211 **al.** Enhancing stimulation of cyaniding, *GhLDOX3* activates reactive oxygen species to
1212 regulate tolerance of alkalinity negatively in cotton. Ecotox Environ Safe.
1213 2023:**267**:115655. https://doi.org/10.1016/j.ecoenv.2023.115655
1214 **Kamibayashi C, Lickteig RL, Estes R, Walter G, Mumby MC.** Expression of the A
1215 subunit of protein phosphatase 2A and characterization of its interactions with the

catalytic and regulatory subunits. J Biol Chem. 1992:**267**(30):21864-21872. https://doi.org/10.1016/s0021-9258(19)36692-x

Kerchev P, Waszczak C, Lewandowska A, Willems P, Shapiguzov A, Li Z, Alseekh S, Muhlenbock P, Hoeberichts FA, Huang J, et al. Lack of GLYCOLATE OXIDASE1, but Not GLYCOLATE OXIDASE2, Attenuates the Photorespiratory Phenotype of CATALASE2-Deficient Arabidopsis. Plant Physiol. 2016:**171**(3):1704-1719. https://doi.org/10.1104/pp.16.00359

Koes R, Verweij W, Quattrocchio F. Flavonoids: a colorful model for the regulation and evolution of biochemical pathways. Trends Plant Sci. 2005:**10**(5):236-242. https://doi.org/10.1016/j.tplants.2005.03.002

Kovtun Y, Chiu WL, Tena G, Sheen J. Functional analysis of oxidative stress-activated mitogen-activated protein kinase cascade in plants. Proc Natl Acad Sci U S A. 2000:**97**(6):2940-2945. https://doi.org/10.1073/pnas.97.6.2940

Landi M, Tattini M, Gould KS. Multiple functional roles of anthocyanins in plant-environment interactions. Environ Exp Bot. 2015:**119**:4-17. https://doi.org/10.1016/j.envexpbot.2015.05.012

Lee DW, Gould KS. Why leaves turn red: pigments called anthocyanins probably protect leaves from light damage by direct shielding and by scavenging free radicals. AM SCI. 2002:**90**(6):524-531. https://doi.org/10.1511/2002.6.524

Lesk C, Rowhani P, Ramankutty N. Influence of extreme weather disasters on global

crop production. Nature. 2016:**529**(7584):84-87. https://doi.org/10.1038/nature16467

Li Y, Wang Y, Tan S, Li Z, Yuan Z, Glanc M, Domjan D, Wang K, Xuan W, Guo Y, et al. Root Growth Adaptation is Mediated by PYLs ABA Receptor-PP2A Protein Phosphatase Complex. Adv Sci. 2020:**7**(3):1901455. https://doi.org/10.1002/advs.201901455

Li YY, Mao K, Zhao C, Zhao XY, Zhang HL, Shu HR, Hao YJ. MdCOP1 ubiquitin E3 ligases interact with MdMYB1 to regulate light-induced anthocyanin biosynthesis and red fruit coloration in apple. Plant Physiol. 2012:**160**(2):1011-1022. https://doi.org/10.1104/pp.112.199703

Lillo C, Kataya AR, Heidari B, Creighton MT, Nemie-Feyissa D, Ginbot Z, Jonassen EM. Protein phosphatases PP2A, PP4 and PP6: mediators and regulators in development and responses to environmental cues. Plant Cell Environ. 2014:**37**(12):2631-2648. https://doi.org/10.1111/pce.12364

Lin-Wang K, Micheletti D, Palmer J, Volz R, Lozano L, Espley R, Hellens RP, Chagne D, Rowan DD, Troggio M, et al. High temperature reduces apple fruit colour via modulation of the anthocyanin regulatory complex. Plant Cell Environ. 2011:**34**(7):1176-1190. https://doi.org/10.1111/j.1365-3040.2011.02316.x

Livak KJ, Schmittgen TD. Analysis of relative gene expression data using real-time quantitative PCR and the $2^{-\triangle\triangle C_T}$ method. Methods. 2001:**25**(4):402-408. https://doi.org/10.1006/meth.2001.1262

Mine A, Berens ML, Nobori T, Anver S, Fukumoto K, Winkelmuller TM, Takeda A, Becker D, Tsuda K. Pathogen exploitation of an abscisic acid- and jasmonate-inducible MAPK phosphatase and its interception by *Arabidopsis* immunity. Proc Natl Acad Sci U S A. 2017:**114**(28):7456-7461. https://doi.org/10.1073/pnas.1702613114

Mittler R. ROS Are Good. Trends Plant Sci. 2017:**22**(1):11-19. https://doi.org/10.1016/j.tplants.2016.08.002

Mittler R, Zandalinas SI, Fichman Y, Van Breusegem F. Reactive oxygen species signalling in plant stress responses. Nat Rev Mol Cell Biol. 2022:**23**(10):663-679. https://doi.org/10.1038/s41580-022-00499-2

Nakabayashi R, Yonekura-Sakakibara K, Urano K, Suzuki M, Yamada Y, Nishizawa T, Matsuda F, Kojima M, Sakakibara H, Shinozaki K, et al. Enhancement of oxidative and drought tolerance in Arabidopsis by overaccumulation of antioxidant flavonoids. Plant J. 2014:**77**(3):367-379. https://doi.org/10.1111/tpj.12388

Neill SO, Gould KS, Kilmartin PA, Mitchell KA, Markham KR. Antioxidant activities of red versus green leaves in *Elatostema rugosum*. Plant Cell Environ. 2002:**25**(4):539-547. https://doi.org/10.1046/j.1365-3040.2002.00837.x

Ni J, Wang S, Yu W, Liao Y, Pan C, Zhang M, Tao R, Wei J, Gao Y, Wang D, et al. The ethylene-responsive transcription factor PpERF9 represses *PpRAP2.4* and

PpMYB114 via histone deacetylation to inhibit anthocyanin biosynthesis in pear. Plant Cell. 2023:**35**(6):2271-2292. https://doi.org/10.1093/plcell/koad077

Olsson AS, Engström P, Söderman E. The homeobox genes *ATHB12* and *ATHB7* encode potential regulators of growth in response to water deficit in *Arabidopsis*. Plant Mol Biol. 2004:**55**(5):663-677. https://doi.org/10.1007/s11103-004-1581-4

Qu Y, Bai X, Zhu YJ, Qi R, Tian G, Wang Y, Li YH, Zhang KM. Reactive Oxygen Species Acts as an Important Inducer in Low-temperature-induced Anthocyanin Biosynthesis in *Begonia semperflorens*. J Am Soc Hortic Sci. 2018:**143**(6):486-493. https://doi.org/10.21273/JASHS04488-18

Ren H, Rao J, Tang M, Li Y, Dang X, Lin D. PP2A interacts with KATANIN to promote microtubule organization and conical cell morphogenesis. J Integr Plant Biol. 2022:**64**(8):1514-1530. https://doi.org/10.1111/jipb.13281

Ruediger R, Hentz M, Fait J, Mumby M, Walter G. Molecular model of the A subunit of protein phosphatase 2A interaction with other subunits and tumor antigens. J Virol. 1994:**68**(1):123-129. https://doi.org/10.1128/JVI.68.1.123-129.1994

Schaart JG, Dubos C, De La Fuente IR, van Houwelingen AMML, de Vos RCH, Jonker HH, Xu WJ, Routaboul JM, Lepiniec L, Bovy AG. Identification and characterization of MYB‐bHLH‐WD40 regulatory complexes controlling proanthocyanidin biosynthesis in strawberry (*Fragaria* × *ananassa*) fruits. New Phytol. 2012:**197**(2):454-467. https://doi.org/10.1111/nph.12017

Shan X, Zhang Y, Peng W, Wang Z, Xie D. Molecular mechanism for jasmonate-induction of anthocyanin accumulation in *Arabidopsis*. J Exp Bot. 2009:**60**(13):3849-3860. https://doi.org/10.1093/jxb/erp223

Shi H, Liu G, Wei Y, Chan Z. The zinc-finger transcription factor ZAT6 is essential for hydrogen peroxide induction of anthocyanin synthesis in *Arabidopsis*. Plant Mol Biol. 2018:**97**(1-2):165-176. https://doi.org/10.1007/s11103-018-0730-0

Soderman E, Mattsson J, Engstrom P. The *Arabidopsis* homeobox gene *ATHB-7* is induced by water deficit and by abscisic acid. Plant J. 1996:**10**(2):375-381. https://doi.org/10.1046/j.1365-313x.1996.10020375.x

Söderman E, Hjellström M, Fahleson J, Engström P. The HD-Zip gene *ATHB6* in *Arabidopsis* is expressed in developing leaves, roots and carpels and up-regulated by water deficit conditions. Plant Mol Biol. 1999:**40**(6):1073-1083. https://doi.org/10.1023/A:1006267013170

Steyn WJ, Wand SJE, Holcroft DM, Jacobs G. Anthocyanins in vegetative tissues: a proposed unified function in photoprotection. New Phytol. 2002:**155**(3):349-361. https://doi.org/10.1046/j.1469-8137.2002.00482.x

Takos AM, Jaffe FW, Jacob SR, Bogs J, Robinson SP, Walker AR. Light-induced expression of a *MYB* gene regulates anthocyanin biosynthesis in red apples. Plant Physiol. 2006:**142**(3):1216-1232. https://doi.org/10.1104/pp.106.088104

Uhrig RG, Labandera AM, Moorhead GB. *Arabidopsis* PPP family of serine/threonine

protein phosphatases: many targets but few engines. Trends Plant Sci. 2013:**18**(9):505-513. https://doi.org/10.1016/j.tplants.2013.05.004

Wang L, Leister D, Guan L, Zheng Y, Schneider K, Lehmann M, Apel K, Kleine T. The *Arabidopsis* SAFEGUARD1 suppresses singlet oxygen-induced stress responses by protecting grana margins. Proc Natl Acad Sci U S A. 2020:**117**(12):6918-6927. https://doi.org/10.1073/pnas.1918640117

Winkel-Shirley B. Flavonoid biosynthesis. A colorful model for genetics, biochemistry, cell biology, and biotechnology. Plant Physiol. 2001:**126**(2):485-493. https://doi.org/10.1104/pp.126.2.485

Xie XB, Li S, Zhang RF, Zhao J, Chen YC, Zhao Q, Yao YX, You CX, Zhang XS, Hao YJ. The bHLH transcription factor MdbHLH3 promotes anthocyanin accumulation and fruit colouration in response to low temperature in apples. Plant Cell Environ. 2012:**35**(11):1884-1897. https://doi.org/10.1111/j.1365-3040.2012.02523.x

Xu H, Zou Q, Yang G, Jiang S, Fang H, Wang Y, Zhang J, Zhang Z, Wang N, Chen X. MdMYB6 regulates anthocyanin formation in apple both through direct inhibition of the biosynthesis pathway and through substrate removal. Hortic Res. 2020:**7**(1):72. https://doi.org/10.1038/s41438-020-0294-4

Xu W, Dubos C, Lepiniec L. Transcriptional control of flavonoid biosynthesis by MYB-bHLH-WDR complexes. Trends Plant Sci. 2015:**20**(3):176-185. https://doi.org/10.1016/j.tplants.2014.12.001

Xu Z, Mahmood K, Rothstein SJ. ROS Induces Anthocyanin Production Via Late Biosynthetic Genes and Anthocyanin Deficiency Confers the Hypersensitivity to ROS-Generating Stresses in Arabidopsis. Plant Cell Physiol. 2017:**58**(8):1364-1377. https://doi.org/10.1093/pcp/pcx073

Zhang D, Yu B, Bai J, Qian M, Shu Q, Su J, Teng Y. Effects of high temperatures on UV-B/visible irradiation induced postharvest anthocyanin accumulation in 'Yunhongli No. 1' (*Pyrus pyrifolia* Nakai) pears. Sci Hortic. 2012:**134**:53-59. https://doi.org/10.1016/j.scienta.2011.10.025

Zhang L, Tao R, Wang S, Gao Y, Wang L, Yang S, Zhang X, Yu W, Wu X, Li K, et al. PpZAT5 suppresses the expression of a B-box gene *PpBBX18* to inhibit anthocyanin biosynthesis in the fruit peel of red pear. Front Plant Sci. 2022:**13**:1022034. https://doi.org/10.3389/fpls.2022.1022034

Zhou HW, Nussbaumer C, Chao Y, DeLong A. Disparate roles for the regulatory A subunit isoforms in Arabidopsis protein phosphatase 2A. Plant Cell. 2004:**16**(3):709-722. https://doi.org/10.1105/tpc.018994

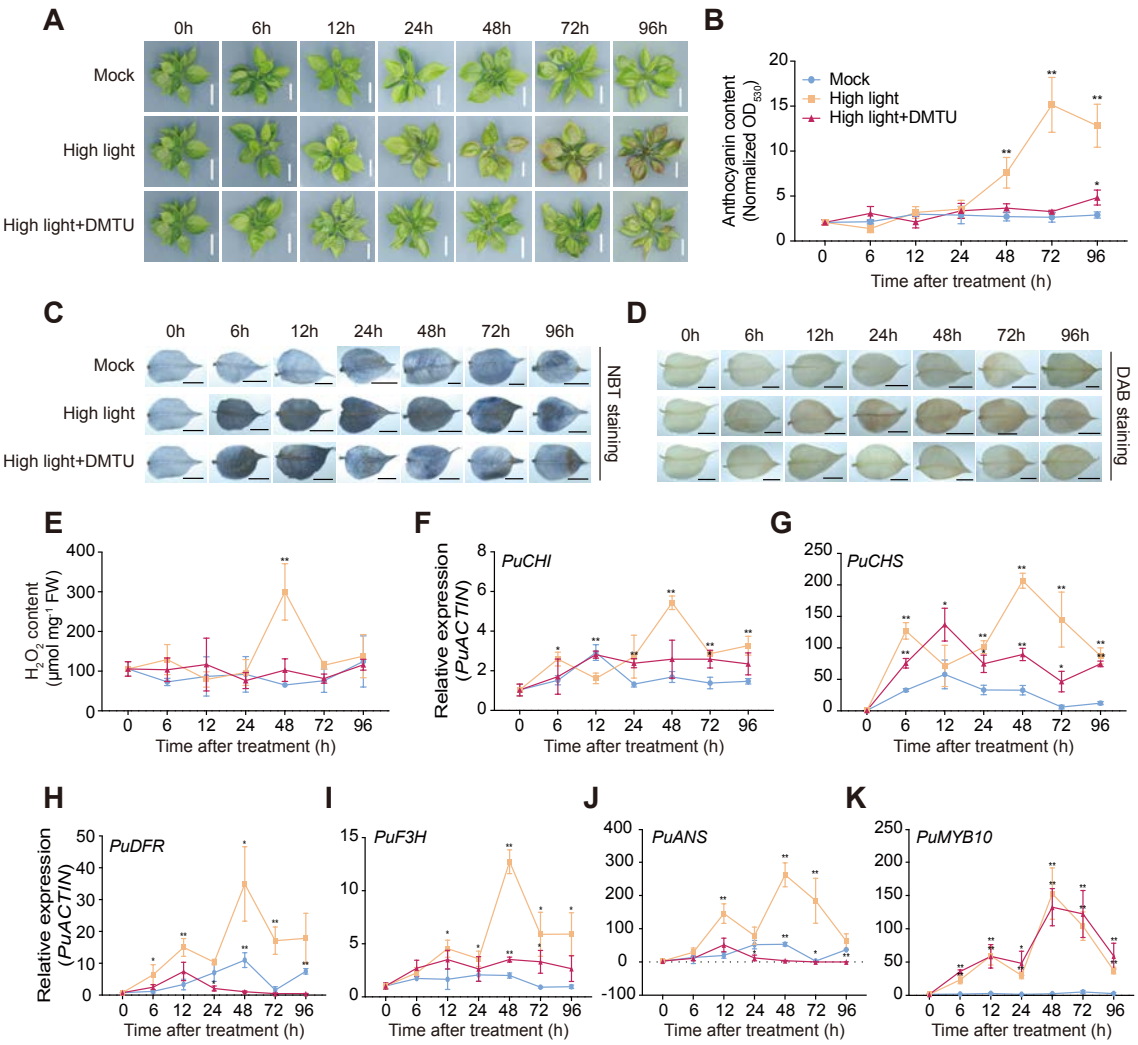

Figure 1. High light stress-induced anthocyanin biosynthesis is ROS-dependent. A-K), Pear seedlings were treated with high light stress treatment (photon flux density: approximately 160 μmol·s^{-1}·m^{-2}) or high light stress supplemented with N, N'-dimethylthiourea (DMTU) treatment. DMTU was applied as ROS scavenger, and pear seedlings under appropriate light condition were used as Mock (photon flux density: approximately 50 μmol·s^{-1}·m^{-2}). Pear seedlings were sampled at 0 h, 6 h, 12 h, 24 h, 48 h, 72 h, 96 h. **A)**, Phenotype of pear seedlings (scale bar, 1 cm). **B)**, The anthocyanin content for pear seedlings. **C and D)**, NBT staining for superoxide and DAB staining for H2O2 in pear seedlings leaves, respectively (scale bar, 0.5 mm). **E)**, H2O2 quantification of pear seedlings. **F-K)**, The expression levels of *PuCHI*, *PuCHS*, *PuDFR*, *PuF3H*, *PuANS*, *PuMYB10* in pear seedlings under different treatments. *PuACTIN* was amplified as an internal control. Data are presented as means ± s.d. of 3 biological replicates. Asterisks indicate significant differences compared with Mock group (two-tailed Student's t-test, *P < 0.05, **P < 0.01), all exact P values are shown in Supplemental Data Set S5.

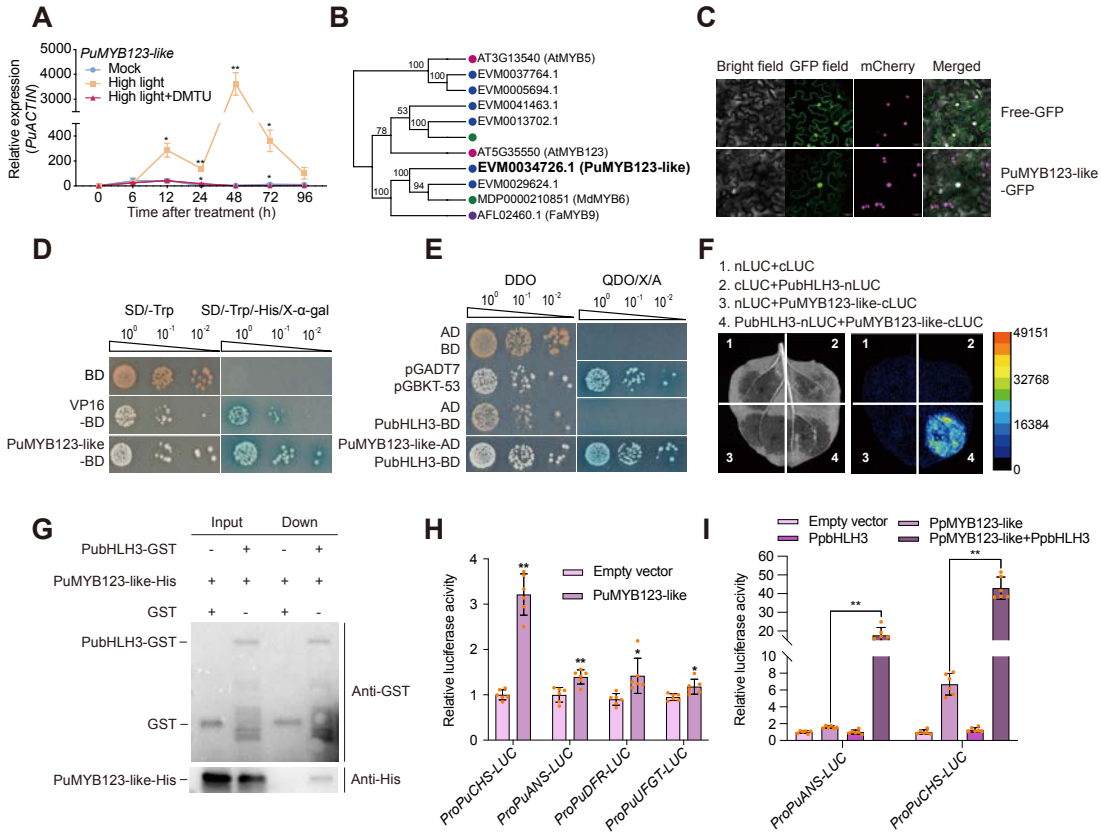

Figure 2. Identification of PuMYB123-like and its interaction with PubHLH3. A) The expression levels of *PuMYB123-like* in pear seedlings under high-light stress treatment or high-light stress supplemented with DMTU treatment, and pear seedlings under appropriate light condition were used as Mock. *PuACTIN* was amplified as an internal control. **B)** Phylogenetic analysis of PuMYB123-like. The phylogenetic tree was generated using the Maximum-likelihood method of MEGA (version 10.1.8). Bootstrap values from 1000 replicates for each branch are shown. The protein sequences from pear (Pu, *Pyrus pyrifolia*, highlighted with blue dots), apple (Md, *Malus* × *domestica*, highlighted with green dots), Arabidopsis (At, *Arabidopsis thaliana*, highlighted with rose red dots) and strawberry (Fa, *Fragaria* × *ananassa*, highlighted with purple dots). PuMYB123-like (EVM0034726.1) is bolded and enlarged. **C)** Subcellular localization of PuMYB123-like in *N. benthamiana* leaf cells (scale bar, 25 μm). **D)** Trans-acting activity of PuMYB123-like in yeast cells. **E)** Interaction between PuMYB123-like and PubHLH3 in a yeast two-hybrid assay, with pGADT7-T and pGBKT7-53 as positive controls. DDO, SD/-Trp/-Leu medium; QDO/X/A, SD/-Trp/-Leu/-Ade/-His medium with X-α-gal and Aureobasidin. **F)** The interaction between PuMYB123-like and PubHLH3 was detected by luciferase complementation imaging assays. The pseudocolour scale bar indicates the range of luminescence intensity. **G)** The interaction between PuMYB123-like and PubHLH3 analyzed using a pull-down assay. PuMYB123-like-His was incubated with GST or PubHLH3-GST. The interaction proteins were precipitated by GST-Trap agarose beads and analysed by immunoblotting with an anti-GST or anti-His antibody. **H)** A dual-luciferase assay demonstrated that PuMYB123-like promotes the promoter activity of anthocyanin-related genes (*PuCHS, PuANS, PuDFR, PuUFGT*). The promoter of anthocyanin-related genes was cloned into the pGreenII 0800-LUC (firefly luciferase) vector, and the full-length CDS of *PuMYB123-like* was cloned into the pGreenII 0029 62-SK vector. The empty vector of pGreenII 0029 62-SK was used as control. **I)** Dual-luciferase assay showed that interaction between PuMYB123-like and PubHLH3 significantly enhanced activation of PuMYB123-like on *PuCHS* and *PuANS* promoters. Data are presented as means ± s.d. of 3 biological replicates **A)** and 6 biological replicates **H)** and **I)**. Asterisks indicate significant differences compared with Mock **A)**, empty vector **H)** and PuMYB123-like **I)** (two-tailed Student's t-test, *P < 0.05, **P < 0.01), all exact P values are shown in Supplemental Data Set S5.

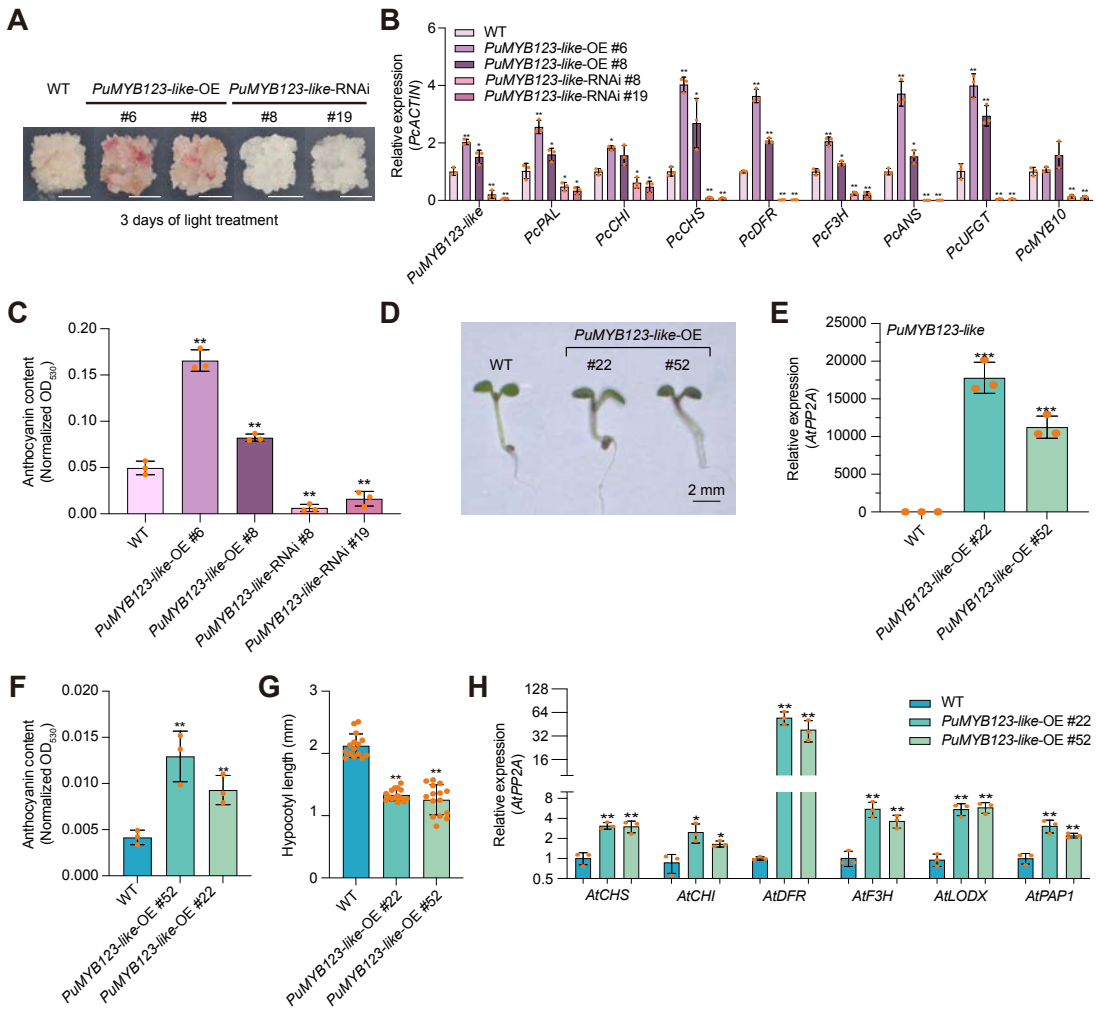

Figure 3. PuMYB123-like promotes anthocyanin biosynthesis. A) Phenotype of pear calli overexpressing and silencing *PuMYB123-like* (scale bar, 1 cm). Wild type pear calli were used as the negative control. Pear calli were incubated under continuous white light at 17°C for 3 d. **B)** Expression levels of anthocyanin-related genes and *PuMYB123-like* in *PuMYB123-like*-OE *and PuMYB123-like*-RNAi pear calli after light treatment. *PcACTIN* was amplified as an internal control. **C)** Anthocyanin contents in *PuMYB123-like*-OE and *PuMYB123-like*-RNAi pear calli after light treatment. **D)** Phenotype of *Arabidopsis* seedlings overexpressing *PuMYB123-like* (scale bar, 2 mm). Wild-type 'Columbia 0' was used as the negative control. *Arabidopsis* seedlings were grown on 1/2 MS medium for 5 days. **E)** Expression levels of *PuMYB123-like* in transgenic *Arabidopsis* lines. *AtPP2A* was amplified as an internal control. **F)** Anthocyanin contents in transgenic *Arabidopsis* lines. **G)** The hypocotyl length of transgenic *Arabidopsis* seedlings. **H)** Expression levels of anthocyanin-related genes in transgenic *Arabidopsis* lines. Data are presented as means ± s.d. of 3 biological replicates **B)**, **C)**, **E)**, **F)** and **H)** and 15 biological replicates **G)**. Asterisks indicate significant differences compared with wild type pear calli **B)** and **C)**, wild type *Arabidopsis* **E-H)**, (two-tailed Student's *t-test*, $*P < 0.05$, $**P < 0.01$), all exact *P* values are shown in Supplemental Data Set S5.

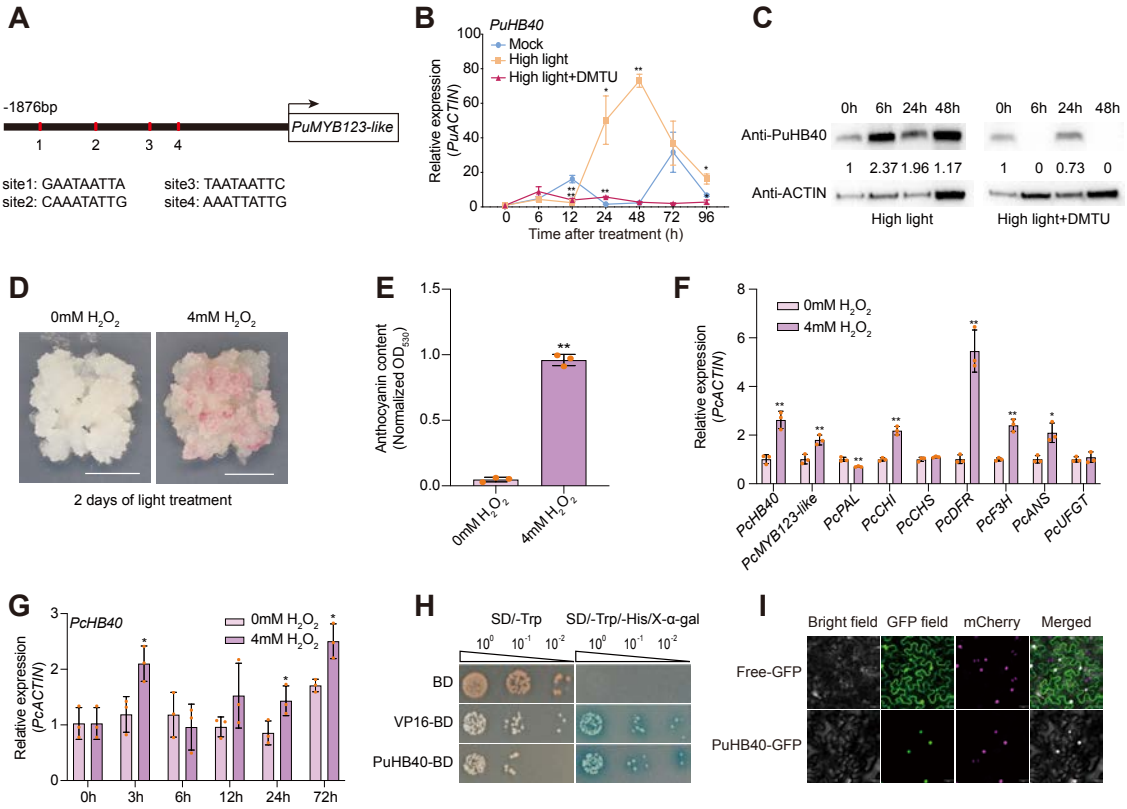

Figure 4. Identification of PuHB40 and its response to ROS. **A)** Distribution of potential binding sites of PuHB40 in *PuMYB123-like* promoter region. Vertical red lines indicate the position of site1 to site4. **B)** The expression levels of *PuHB40* in pear seedlings under high-light stress treatment or high-light stress supplemented with DMTU treatment, and pear seedlings under appropriate light condition were used as Mock. *PuACTIN* was amplified as an internal control. **C)** Changes in the PuHB40 abundance in pear seedlings under high-light stress treatment or high-light stress supplemented with DMTU treatment for 0 h, 6 h, 24 h, 48 h. The PuHB40 protein was detected by immunoblotting with an affinity-purified specific anti-PuHB40 polyclonal antibody. **D)** Phenotype of pear calli after 4 mM H_2O_2 treatment for 2 days (scale bar, 1 cm). Pear calli treated with 0 mM H_2O_2 were used as control. **E)** Anthocyanin contents in pear calli treated with 0 mM or 4 mM H_2O_2 for 2 days. **F)** Expression levels of *PcHB40*, *PcMYB123-like* and anthocyanin-related genes in pear calli treated with 0 mM or 4 mM H_2O_2 for 2 days. *PcACTIN* was amplified as an internal control. **G)** Expression levels of *PcHB40* in pear calli after 0 mM or 4 mM H_2O_2 treatment for 0 h, 3 h, 6 h, 12 h, 24 h, 72 h. *PcACTIN* was amplified as an internal control. **H)** Trans-acting activity of PuHB40 in yeast cells. **I)** Subcellular localization of PuHB40 in *N. benthamiana* leaf cells (scale bar, 25 μm). Data are presented as means ± s.d. of 3 biological replicates. Asterisks indicate significant differences compared with Mock **B)**, 4 mM H_2O_2 **E-F)** (two-tailed Student's *t-test*, $*P < 0.05$, $**P < 0.01$), all exact *P* values are shown in Supplemental Data Set S5.

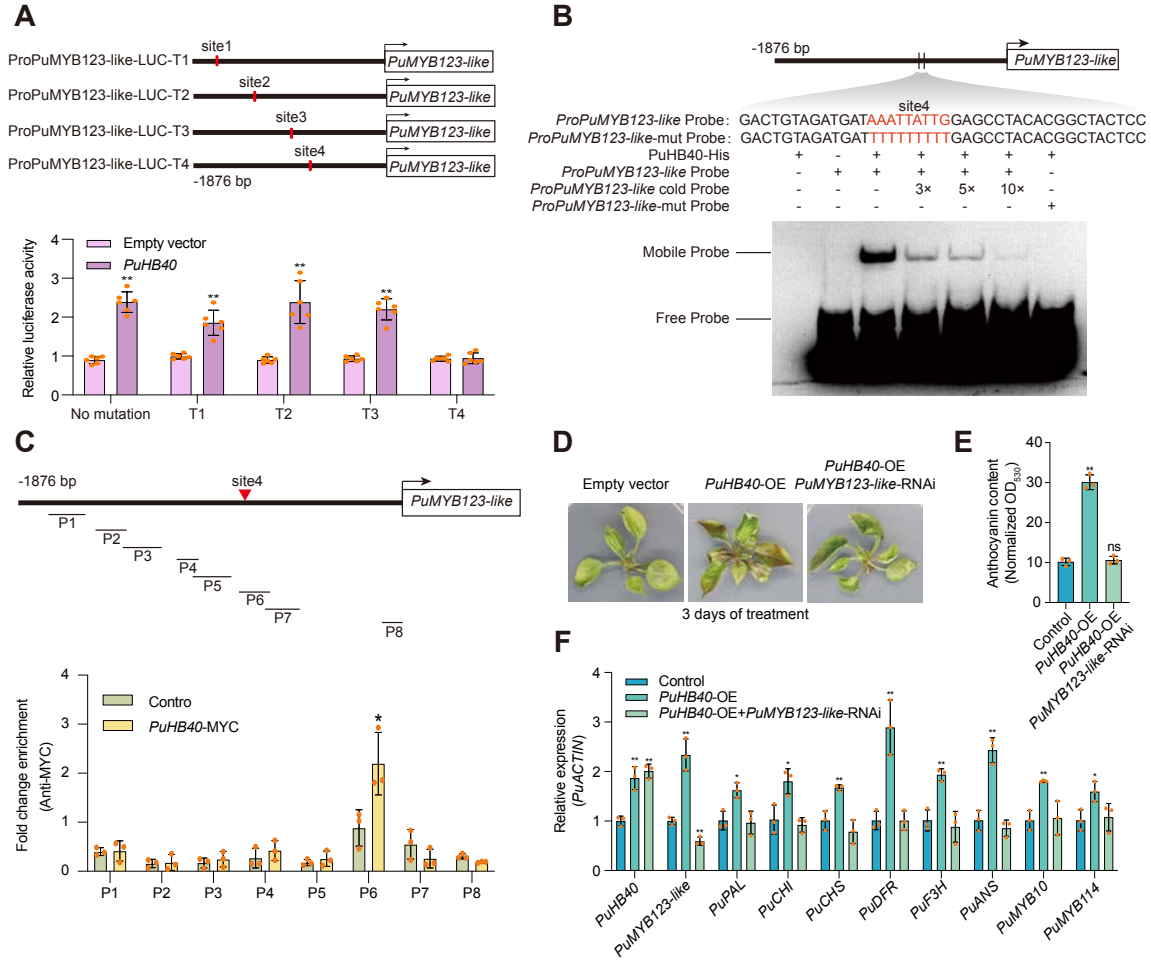

Figure 5. PuHB40 positively regulates anthocyanin biosynthesis by promoting *PuMYB123-like* transcription. A) Effect of potential binding sites mutation on the activation of *PuMYB123-like* by PuHB40. Four potential binding sites (site1 to site4) were mutated into TTTTTTTTT, respectively. The promoters of *PuMYB123-like* with or without potential binding site mutation were cloned into the pGreenII 0800-LUC (firefly luciferase) vector, and the full-length CDS of *PuHB40* was cloned into the pGreenII 0029 62-SK vector. The empty vector of pGreenII 0029 62-SK was used as control. **B)** An EMSA confirmed that PuHB40 binds directly to the site4 in the *PuMYB123-like* promoter. The *ProPuMYB123-like* probe was the biotin-labeled fragment of *PuMYB123-like* promoter containing site4 (AAATTATTG), whereas the cold probe was an unlabeled probe (50-, 100-, and 200-fold molar excess). *ProPuMYB123-like*-mut probe was the same as the *ProPuMYB123-like* probe but with site4 (AAATTATTG) mutated to TTTTTTTTT. The His-tagged PuHB40 protein was purified. **C)** ChIP-qPCR assay results reflected the in vivo

binding of PuHB40 to the *PuMYB123-like* promoter. Cross-linked chromatin samples were extracted from *PuHB40*-MYC-overexpressing pear calli with 3 biological replicates and precipitated with an anti-MYC antibody. Eluted DNA was used to amplify *PuMYB123-like* promoter fragments and eight regions (P1 to P8) were examined, among which P6 containing site4. Pear calli overexpressing the MYC sequence were used as a negative control. Three biological replicates of pear calli were used in the ChIP assay. **D)** Transient overexpression of *PuHB40* with or without transient silencing of *PuMYB123-like* in pear seedlings. The full-length CDS of *PuHB40* and reverse complementary gene fragment (~200 to 300 bp) of *PuMYB123-like* were inserted into the pCAMBIA1301 vector for the subsequent expression under the control of the 35S promoter. The plasmids were transformed into *A. tumefaciens* GV3101 and infiltrated into pear seedlings by vacuum. The infiltrated pear seedlings were firstly incubated in darkness for 2 days and then exposed to continuous white light for 3 days. Pear seedlings infiltrated with an empty pCAMBIA1301 vector were used as a control. **E)** Anthocyanin content in pear seedlings. **F)** Expression levels of *PuHB40*, *PuMYB123-like* and anthocyanin-related genes in pear seedlings. Data are presented as means ± s.d. of 3 biological replicates **C), E)**, **F)** and 6 biological replicates **A)**. Asterisks indicate significant differences compared with empty vector **A)** and control **C), E)**, **F)** (two-tailed Student's *t-test*, $*P < 0.05$, $**P < 0.01$; ns, no significance, $P > 0.05$), all exact P values are shown in Supplemental Data Set S5.

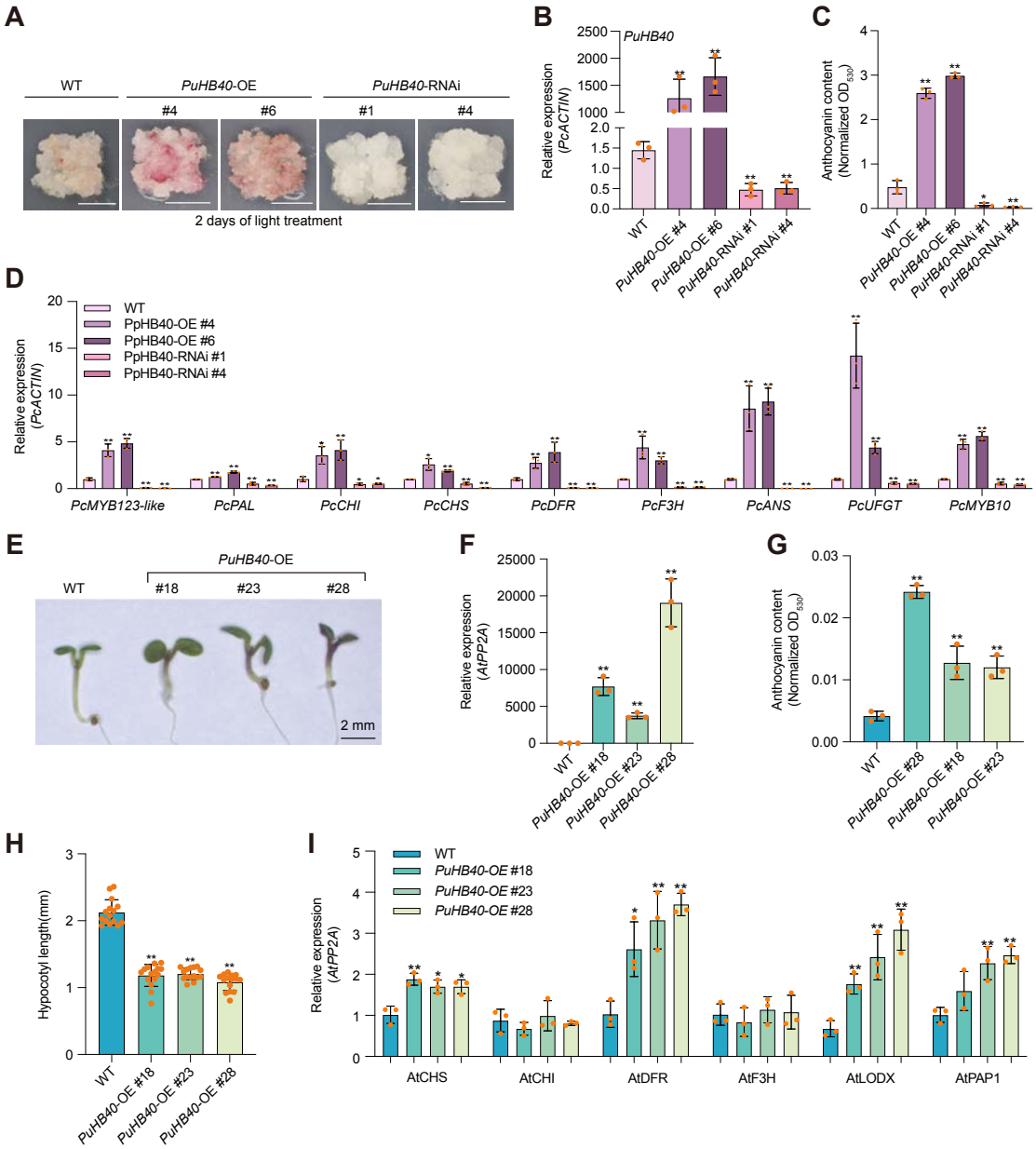

Figure 6. PuHB40 promotes anthocyanin biosynthesis. A) Phenotype of pear calli overexpressing and silencing *PuHB40* (scale bar, 1 cm). Wild type pear calli were used as the negative control. Pear calli were incubated under continuous white light at 17°C for 3 d. **B)** and **D)** Expression levels of *PuHB40*, *PpMYB123-like* and anthocyanin-related genes in *PuHB40*-OE and *PuHB40*-RNAi pear calli after light treatment. *PcACTIN* was amplified as an internal control. **C)** Anthocyanin contents in *PuHB40*-OE and *PuHB40*-RNAi pear calli after light treatment. **E)** Phenotype of *Arabidopsis* seedlings overexpressing *PuHB40* (scale bar, 2 mm). Wild-type 'Columbia 0' was used as the negative control. *Arabidopsis* seedlings were grown on 1/2 MS medium for 5 days. **F)** Expression levels of *PuHB40* in transgenic *Arabidopsis* lines. *AtPP2A* was amplified as an internal control. **G)** Anthocyanin contents in transgenic *Arabidopsis* lines. **H)** The hypocotyl length of transgenic *Arabidopsis* seedlings. **I)** Expression levels of anthocyanin-related genes in transgenic *Arabidopsis* lines. Data are presented as means ± s.d. of 3 biological replicates **B-D)**, **F)**, **G)**, **I)** and 15 biological replicates **H)**. Asterisks indicate significant differences compared with wild type pear calli **B-D)** and wild type *Arabidopsis* **F-I)** (two-tailed Student's *t-test*, $*P < 0.05$, $**P < 0.01$), all exact *P* values are shown in Supplemental Data Set S5.

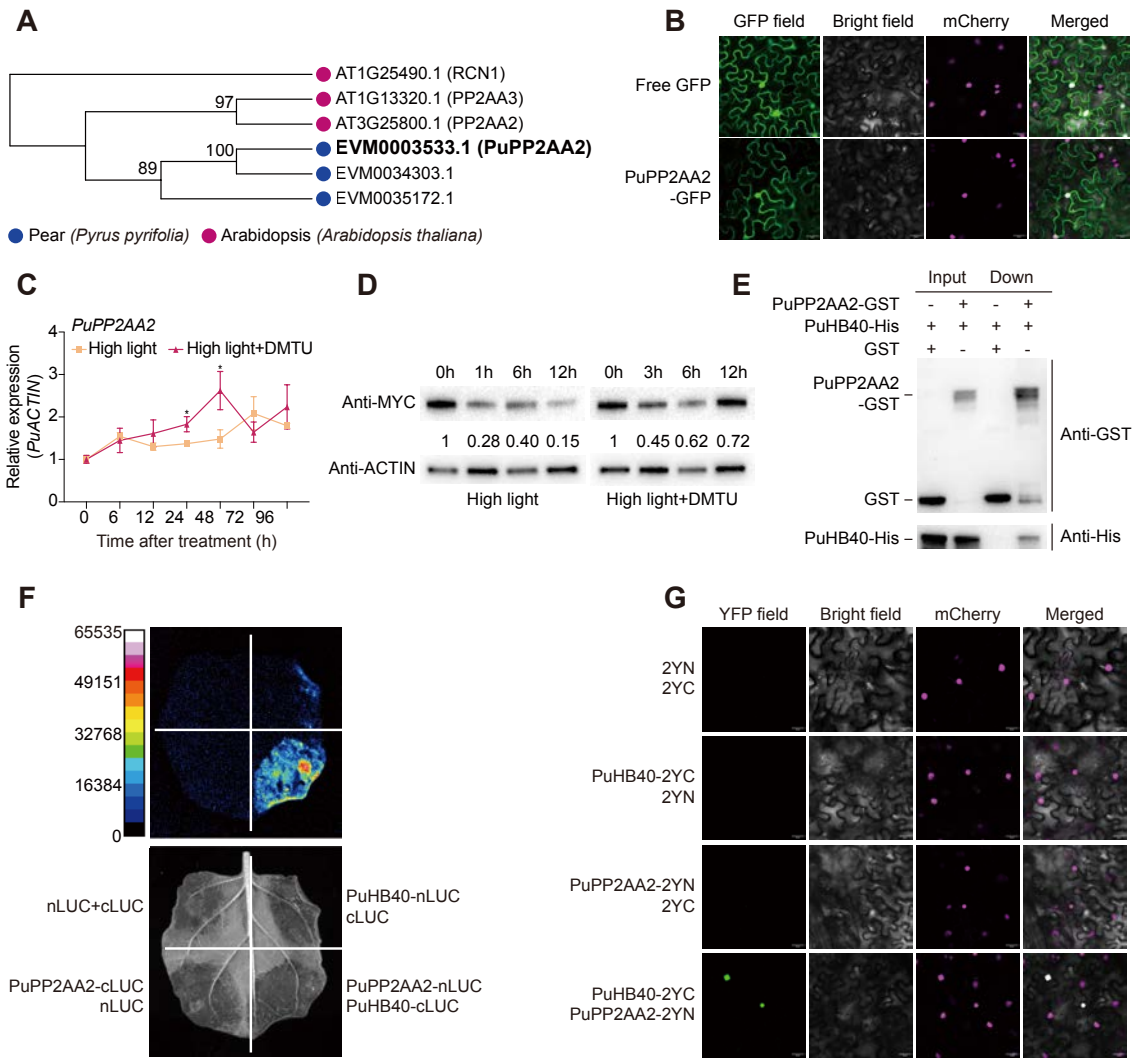

Figure 7. Identification of PuPP2AA2 and its interaction with PuHB40. A) Phylogenetic analysis of PuPP2AA2. The phylogenetic tree was generated using the Maximum-likelihood method of MEGA (version 10.1.8). Bootstrap values from 1000 replicates for each branch are shown. The protein sequences from pear (Pu, *Pyrus pyrifolia*, highlighted with blue dots) and Arabidopsis (*Arabidopsis thaliana*, highlighted with rose red dots). PuPP2AA2 (EVM0003533.1) is bolded and enlarged. **B)** Subcellular localization of PuPP2AA2 in *N. benthamiana* leaf cells (scale bar, 25 μm). **C)** The expression levels of *PuPP2AA2* in pear seedlings under high-light stress treatment or high-light stress supplemented with DMTU treatment. *PuACTIN* was amplified as an internal control. **D)** Changes in the PuPP2AA2 abundance in pear seedlings. Pear seedlings transiently overexpressed MYC-tagged *PuPP2AA2* and were exposed to high-light stress treatment or high-light stress supplemented with DMTU treatment for 0 h, 3 h, 6 h, 12 h. The PuPP2AA2 protein was detected by immunoblotting with anti-MYC monoclonal antibody. **E)** The interaction between PuPP2AA2 and PuHB40 using a pull-down assay. PuHB40-His was incubated with GST or PuPP2AA2-GST. The interaction proteins were precipitated by GST-Trap agarose beads and analysed by immunoblotting with an anti-GST or anti-His antibody. **F)** The interaction between PuPP2AA2 and PuHB40 was detected by luciferase complementation imaging assays. The pseudocolour scale bar indicates the range of luminescence intensity. **G)** Physical association between PuPP2AA2 and PuHB40 confirmed by a BiFC assay. Fluorescence indicates positive interactions (scale bar, 25 μm). Data are presented as means ± s.d. of 3 biological replicates. Asterisks indicate significant differences compared with high-light stress supplemented with DMTU treatment (two-tailed Student's *t-test*, $*P < 0.05$), all exact *P* values are shown in Supplemental Data Set S5.

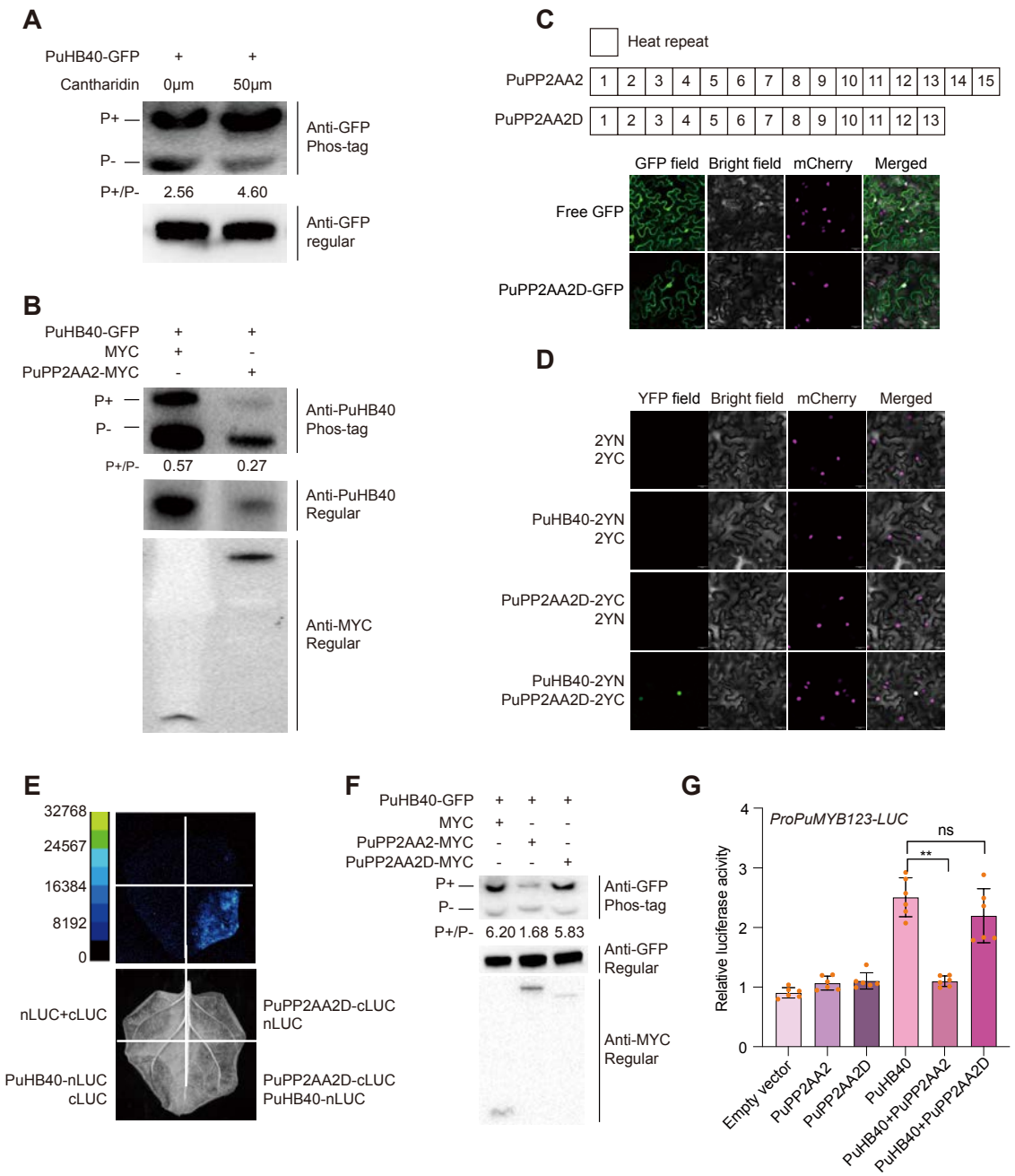

Figure 8. PuHB40 was dephosphorylated by PP2A phosphatase. A) Phos-tag analysis of phosphorylation of PuHB40 after cantharidin treatment. *A. tumefaciens* GV3101 containing PuHB40-GFP plasmid infiltrated into *N. benthamiana* leaves by injection and 50 μM cantharidin was injected into the same position as the agrobacteria after 24 h. *N. benthamiana* leaves injected corresponding concentration of DMSO were used as negative control. Protein samples were extracted from *N. benthamiana* leaves after 24 h and were separated in a Phos-tag gel (upper panel), and PuHB40-GFP with different phosphorylated status was detected using the anti-GFP antibody. Total PuHB40-GFP proteins were analyzed by SDS-PAGE without Phos-tag (indicated as "Regular"), and were detected using anti-GFP antibody. P+ and P- indicate phosphorylated and non-phosphorylated form of PuHB40, respectively. The intensity of the bands was measured with the Image J software and was calculated as the ratio of the P+/P- form. **B)** Immunoblotting analysis showing that the PP2A complex directly dephosphorylates PuHB40 *in vitro*. MYC, PP2A complex, and PuHB40-GFP were immunopurified from pear seedlings transiently overexpressing MYC, PuPP2AA2-MYC, and PuHB40-GFP using MYC-Trap or GFP-Trap, respectively.

After incubation of PP2A complexes with PuHB40-GFP (MYC with PuHB40-GFP was set as control), protein samples in the reaction system were separated in Phos-tag gel (upper panel) and detected using the anti-PuHB40 antibody. The intensity of the bands was measured with the Image J software and calculated as the ratio of the P+/P-. Total proteins in the reaction system were analyzed by SDS-PAGE without Phos-tag (indicated as "Regular"). MYC, PuPP2AA2-MYC, and PuHB40-GFP were set as the loading controls and detected by the anti-MYC or anti-PuHB40 antibody, respectively. **C)** Subcellular localization of PuPP2AA2D in *N. benthamiana* leaf cells (scale bar, 25 μm). PuPP2AA2D is PuPP2AA2 with heat repeats 14 and 15 in the C-terminal deleted. **D)** The interaction between PuPP2AA2D and PuHB40 confirmed by a BiFC assay. Fluorescence indicates positive interactions (scale bar, 25 μm). **E)** The interaction between PuPP2AA2D and PuHB40 was detected by luciferase complementation imaging assays. The pseudocolour scale bar indicates the range of luminescence intensity. **F)** Immunoblotting analysis showing that PP2A dephosphorylates PuHB40 *in vivo*. Protein extracts from *N. benthamiana* leaves co-infiltrated PuHB40-GFP with MYC, PuPP2AA2-MYC, or PuPP2AA2D-MYC were separated in Phos-tag gel (upper panel) and detected using the anti-GFP antibody (MYC with PuHB40-GFP was set as control). The intensity of the bands was measured with the Image J software and calculated the ratio of P+/P−. Total PuHB40-GFP, MYC, PuPP2AA2-MYC and PuPP2AA2D-MYC proteins were analyzed by SDS-PAGE without Phos-tag (indicated as "Regular"). PuHB40-GFP, MYC, PuPP2AA2-MYC and PuPP2AA2D-MYC were set as the loading controls and detected by the anti-GFP or anti-MYC antibody, respectively.
G) Dual-luciferase assay showed that dephosphorylation of PuHB40 by PP2A significantly inhibited the activation of *PuMYB123-like* promoter by PuHB40. The *PuMYB123-like* promoter was cloned into the pGreenII 0800-LUC (firefly luciferase) vector, and the full-length CDS of *PuHB40*, PuPP2AA2 and PuPP2AA2D was cloned into the pGreenII 0029 62-SK vector. The PuHB40 was used as control. Data are presented as means ± s.d. of 6 biological replicates **G)**. Asterisks indicate significant differences compared PuHB40 **G)** (two-tailed Student's *t-test*, $^{**}P < 0.01$; ns, no significance, $P > 0.05$), all exact P values are shown in Supplemental Data Set S5.

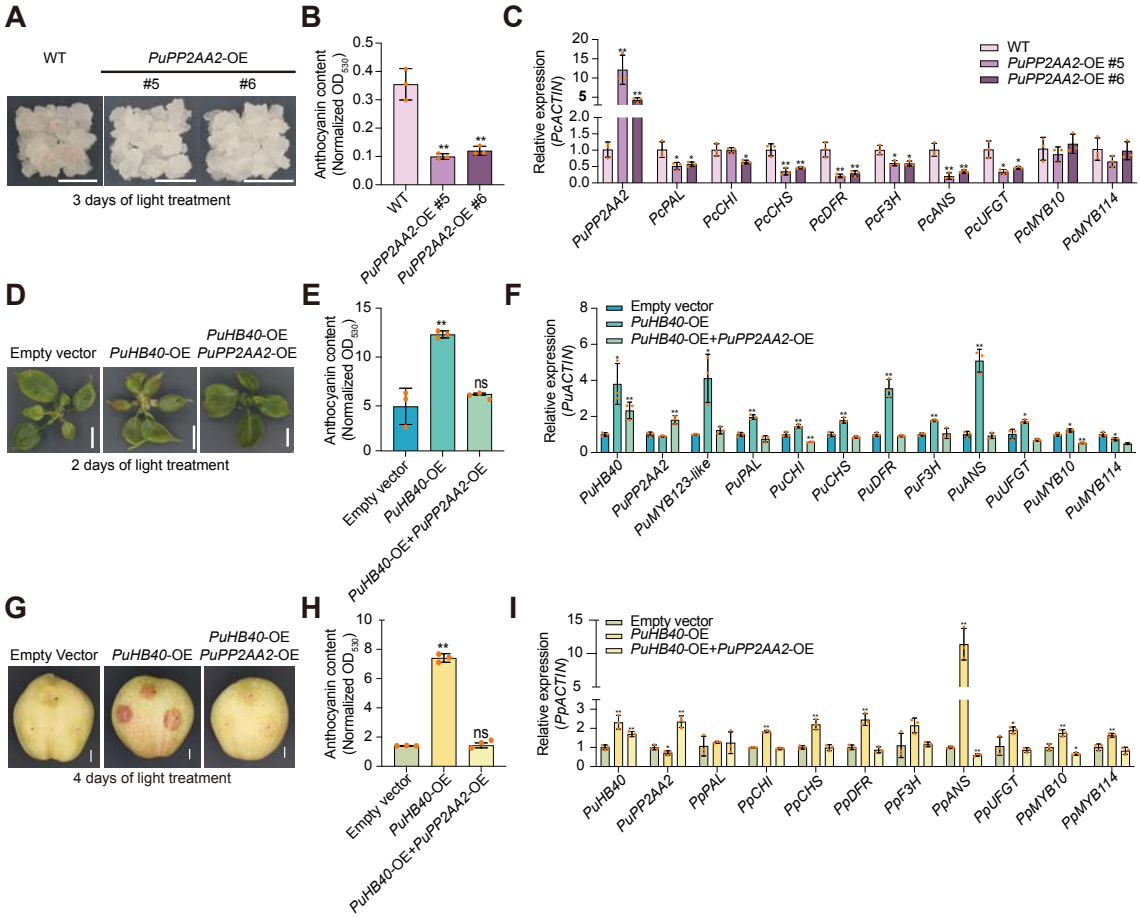

Figure 9. Attenuation of PuHB40-induced anthocyanin biosynthesis by PuPP2AA2. **A)** Phenotype of pear calli overexpressing *PuPP2AA2* (scale bar, 1 cm). Wild type pear calli were used as the negative control. Pear calli were incubated under continuous white light at 17°C for 3 d. **B)** Anthocyanin contents in *PuPP2AA2*-OE after light treatment. **C)** Expression levels of *PuPP2AA2* and anthocyanin-related genes in *PuPP2AA2*-OE pear calli after light treatment. *PcACTIN* was amplified as an internal control. **D)** Transient overexpression of *PuHB40* with or without transient overexpressing of *PuPP2AA2* in pear seedlings. The full-length CDS of *PuHB40* and *PuPP2AA2* were inserted into the pCAMBIA1301 vector for the subsequent expression under the control of the 35S promoter. The plasmids were transformed into *A. tumefaciens* GV3101 and infiltrated into pear seedlings by vacuum. The infiltrated pear seedlings were firstly incubated in darkness for 2 days and then exposed to continuous white light for 3 days. Pear seedlings infiltrated with an empty pCAMBIA1301 vector were used as a control. **E)** Anthocyanin content in pear seedlings. **F)** Expression levels of *PuHB40*, *PuPP2AA2*, *PuMYB123-like* and anthocyanin-related genes in pear seedlings. **G)** Transient overexpression of *PuHB40* with or without transient overexpressing of *PuPP2AA2* in fruit (scale bar, 1 cm). The full-length CDS of *PuHB40* and *PuPP2AA2* were cloned to the pGreenII 0029 62-SK vector for the subsequent expression under the control of the 35S promoter. Pear fruits were infiltrated with *A. tumefaciens* GV3101 cells containing the recombinant plasmid using a needle-free syringe. Fruits infiltrated with an empty pGreenII 0029 62-SK vector were used as a control. The phenotypes were examined after a 1 day dark and 4 days light treatment. **H)** Total anthocyanin content in pear fruits. **I)** Expression levels of *PuHB40*, *PuPP2AA2* and anthocyanin-related genes in pear fruits. Data are presented as means ± s.d. of 3 biological replicates. Asterisks indicate significant differences compared with wild type pear calli **B)** and **C)**, empty vector **E), F), H), I)** (two-tailed Student's *t-test*, $*P < 0.05$, $**P < 0.01$; ns, no significance, $P > 0.05$), all exact P values are shown in Supplemental Data Set S5.

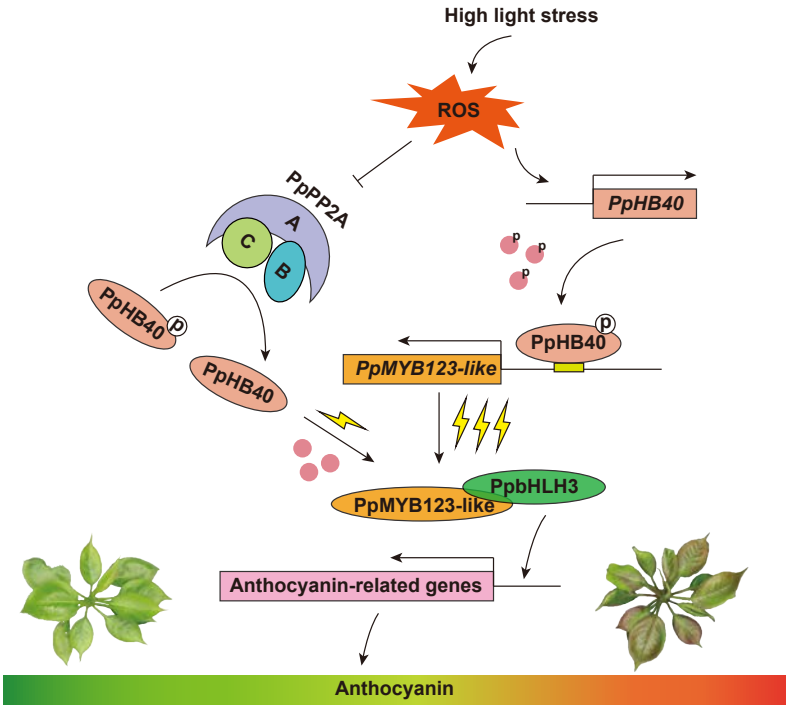

Figure 10. Proposed model for PuHB40-mediated ROS-dependent anthocyanin biosynthesis in pears. PuHB40 is the key transcription factor in ROS-induced anthocyanin biosynthesis. ROS promote PuHB40 expression and then positively regulate its transcriptional activity on PuMYB123-like/PubHLH3 complex to induce anthocyanin biosynthesis. The transcriptional activity of PuHB40 depends on its phosphorylation level which is regulated by PP2A. ROS maintain phosphorylation of PuHB40 at a high level, and enhance the transcriptional activity of PuHB40 on *PuMYB123-like* by reducing the transcriptional and translational levels of PuPP2AA2 under high-light stress, and thus promote anthocyanin biosynthesis. The lightning indicates the intensity of transcriptional regulation of *PuMYB123-like* by PuHB40.

Parsed Citations

Acero N, Gradillas A, Beltran M, Garcia A, Munoz Mingarro D. Comparison of phenolic compounds profile and antioxidant properties of different sweet cherry (Prunus avium L.) varieties. Food Chem. 2019:279:260-271. https://doi.org/10.1016/j.foodchem.2018.12.008
Google Scholar: Author Only Title Only Author and Title

Altangerel N, Ariunbold GO, Gorman C, Alkahtani MH, Borrego EJ, Bohlmeyer D, Hemmer P, Kolomiets MV, Yuan JS, Scully MO. In vivo diagnostics of early abiotic plant stress response via Raman spectroscopy. Proc Natl Acad Sci U S A. 2017:114(13):3393-3396. https://doi.org/10.1073/pnas.1701328114
Google Scholar: Author Only Title Only Author and Title

An JP, Wang XF, Zhang XW, Xu HF, Bi SQ, You CX, Hao YJ. An apple MYB transcription factor regulates cold tolerance and anthocyanin accumulation and undergoes MIEL1-mediated degradation. Plant Biotechnol J. 2020:18(2):337-353. https://doi.org/10.1111/pbi.13201
Google Scholar: Author Only Title Only Author and Title

An XH, Tian Y, Chen KQ, Liu XJ, Liu DD, Xie XB, Cheng CG, Cong PH, Hao YJ. MdMYB9 and MdMYB11 are involved in the regulation of the JA-induced biosynthesis of anthocyanin and proanthocyanidin in apples. Plant Cell Physiol. 2015:56(4):650-662. https://doi.org/10.1093/pcp/pcu205
Google Scholar: Author Only Title Only Author and Title

Ariel FD, Manavella PA, Dezar CA, Chan RL. The true story of the HD-Zip family. Trends Plant Sci. 2007:12(9):419-426. https://doi.org/10.1016/j.tplants.2007.08.003
Google Scholar: Author Only Title Only Author and Title

Bai S, Tao R, Yin L, Ni J, Yang Q, Yan X, Yang F, Guo X, Li H, Teng Y. Two B-box proteins, PpBBX18 and PpBBX21, antagonistically regulate anthocyanin biosynthesis via competitive association with Pyrus pyrifolia ELONGATED HYPOCOTYL 5 in the peel of pear fruit. Plant J. 2019a:100(6):1208-1223. https://doi.org/10.1111/tpj.14510
Google Scholar: Author Only Title Only Author and Title

Bai S, Tao R, Tang Y, Yin L, Ma Y, Ni J, Yan X, Yang Q, Wu Z, Zeng Y, et al. BBX16, a B-box protein, positively regulates light-induced anthocyanin accumulation by activating MYB10 in red pear. Plant Biotechnol J. 2019b:17(10):1985-1997. https://doi.org/10.1111/pbi.13114
Google Scholar: Author Only Title Only Author and Title

Bi X, Zhang J, Chen C, Zhang D, Li P, Ma F. Anthocyanin contributes more to hydrogen peroxide scavenging than other phenolics in apple peel. Food Chem. 2014:152:205-209. https://doi.org/10.1016/j.foodchem.2013.11.088
Google Scholar: Author Only Title Only Author and Title

Bian C, Guo X, Zhang Y, Wang L, Xu T, DeLong A, Dong J. Protein phosphatase 2A promotes stomatal development by stabilizing SPEECHLESS in Arabidopsis. Proc Natl Acad Sci U S A. 2020:117(23):13127-13137. https://doi.org/10.1073/pnas.1912075117
Google Scholar: Author Only Title Only Author and Title

Byrne DP, Shrestha S, Galler M, Cao M, Daly LA, Campbell AE, Eyers CE, Veal EA, Kannan N, Eyers PA. Aurora A regulation by reversible cysteine oxidation reveals evolutionarily conserved redox control of Ser/Thr protein kinase activity. Sci Signal. 2020:13(613). https://doi.org/10.1126/scisignal.aax2713
Google Scholar: Author Only Title Only Author and Title

Catala R, Medina J, Salinas J. Integration of low temperature and light signaling during cold acclimation response in Arabidopsis. Proc Natl Acad Sci U S A. 2011:108(39):16475-16480. https://doi.org/10.1073/pnas.1107161108
Google Scholar: Author Only Title Only Author and Title

Chan KX, Mabbitt PD, Phua SY, Mueller JW, Nisar N, Gigolashvili T, Stroeher E, Grassl J, Arlt W, Estavillo GM, et al. Sensing and signaling of oxidative stress in chloroplasts by inactivation of the SAL1 phosphoadenosine phosphatase. Proc Natl Acad Sci U S A. 2016:113(31):E4567-4576. https://doi.org/10.1073/pnas.1604936113
Google Scholar: Author Only Title Only Author and Title

Choi S, Kwon YR, Hossain MA, Hong S-W, Lee B-h, Lee H. A mutation in ELA1, an age-dependent negative regulator of PAP1/MYB75, causes UV- and cold stress-tolerance in Arabidopsis thaliana seedlings. Plant Sci. 2009:176(5):678-686. https://doi.org/10.1016/j.plantsci.2009.02.010
Google Scholar: Author Only Title Only Author and Title

Croce R, van Amerongen H. Natural strategies for photosynthetic light harvesting. Nat Chem Biol. 2014:10(7):492-501. https://doi.org/10.1038/nchembio.1555
Google Scholar: Author Only Title Only Author and Title

Das PK, Shin DH, Choi SB, Yoo SD, Choi G, Park YI. Cytokinins enhance sugar-induced anthocyanin biosynthesis in Arabidopsis. Mol Cells. 2012:34(1):93-101. https://doi.org/10.1007/s10059-012-0114-2
Google Scholar: Author Only Title Only Author and Title

DeLong A. Switching the flip: protein phosphatase roles in signaling pathways. Curr Opin Plant Biol. 2006:9(5):470-477. https://doi.org/10.1016/j.pbi.2006.07.015
Google Scholar: Author Only Title Only Author and Title

Dubos C, Stracke R, Grotewold E, Weisshaar B, Martin C, Lepiniec L. MYB transcription factors in Arabidopsis. Trends Plant Sci. 2010:15(10):573-581. https://doi.org/10.1016/j.tplants.2010.06.005
Google Scholar: Author Only Title Only Author and Title

Durian G, Rahikainen M, Alegre S, Brosche M, Kangasjarvi S. Protein Phosphatase 2A in the Regulatory Network Underlying Biotic Stress Resistance in Plants. Front Plant Sci. 2016:7:812. https://doi.org/10.3389/fpls.2016.00812
Google Scholar: Author Only Title Only Author and Title

Espley RV, Hellens RP, Putterill J, Stevenson DE, Kutty-Amma S, Allan AC. Red colouration in apple fruit is due to the activity of the MYB transcription factor, MdMYB10. Plant J. 2007:49(3):414-427. https://doi.org/10.1111/j.1365-313X.2006.02964.x
Google Scholar: Author Only Title Only Author and Title

Farkas I, Dombradi V, Miskei M, Szabados L, Koncz C. Arabidopsis PPP family of serine/threonine phosphatases. Trends Plant Sci. 2007:12(4):169-176. https://doi.org/10.1016/j.tplants.2007.03.003
Google Scholar: Author Only Title Only Author and Title

Feild TS, Lee DW, Holbrook NM. Why Leaves Turn Red in Autumn. The Role of Anthocyanins in Senescing Leaves of Red-Osier Dogwood. Plant Physiol. 2001:127(2):566-574. https://doi.org/10.1104/pp.010063
Google Scholar: Author Only Title Only Author and Title

Feng S, Wang Y, Yang S, Xu Y, Chen X. Anthocyanin biosynthesis in pears is regulated by a R2R3-MYB transcription factor PyMYB10. Planta. 2010:232(1):245-255. https://doi.org/10.1007/s00425-010-1170-5
Google Scholar: Author Only Title Only Author and Title

Galvez-Valdivieso G, Fryer MJ, Lawson T, Slattery K, Truman W, Smirnoff N, Asami T, Davies WJ, Jones AM, Baker NR, et al. The high light response in Arabidopsis involves ABA signaling between vascular and bundle sheath cells. Plant Cell. 2009:21(7):2143-2162. https://doi.org/10.1105/tpc.108.061507
Google Scholar: Author Only Title Only Author and Title

Gould KS, McKelvie J, Markham KR. Do anthocyanins function as antioxidants in leaves? Imaging of H2O2 in red and green leaves after mechanical injury. Plant Cell Environ. 2002:25(10):1261-1269. https://doi.org/10.1046/j.1365-3040.2002.00905.x
Google Scholar: Author Only Title Only Author and Title

Groves MR, Hanlon N, Turowski P, Hemmings BA, Barford D. The structure of the protein phosphatase 2A PR65/A subunit reveals the conformation of its 15 tandemly repeated HEAT motifs. Cell. 1999:96(1):99-110. https://doi.org/10.1016/S0092-8674(00)80963-0
Google Scholar: Author Only Title Only Author and Title

Gupta R, Luan S. Redox control of protein tyrosine phosphatases and mitogen-activated protein kinases in plants. Plant Physiol. 2003:132(3):1149-1152. https://doi.org/10.1104/pp.103.020792
Google Scholar: Author Only Title Only Author and Title

Harris JC, Hrmova M, Lopato S, Langridge P. Modulation of plant growth by HD-Zip class I and II transcription factors in response to environmental stimuli. New Phytol. 2011:190(4):823-837. https://doi.org/10.1111/j.1469-8137.2011.03733.x
Google Scholar: Author Only Title Only Author and Title

Himmelbach A, Hoffmann T, Leube M, Hohener B, Grill E. Homeodomain protein ATHB6 is a target of the protein phosphatase ABI1 and regulates hormone responses in Arabidopsis. Embo J. 2002:21(12):3029-3038. https://doi.org/10.1093/emboj/cdf316
Google Scholar: Author Only Title Only Author and Title

Hipsch M, Lampl N, Zelinger E, Barda O, Waiger D, Rosenwasser S. Sensing stress responses in potato with whole-plant redox imaging. Plant Physiol. 2021:187(2):618-631. https://doi.org/10.1093/plphys/kiab159
Google Scholar: Author Only Title Only Author and Title

Hoch WA, Zeldin EL, McCown BH. Physiological significance of anthocyanins during autumnal leaf senescence. Tree Physiol. 2001:21(1):1-8. https://doi.org/10.1093/treephys/21.1.1
Google Scholar: Author Only Title Only Author and Title

Honkanen RE. Cantharidin, another natural toxin that inhibits the activity of serine/threonine protein phosphatases types 1 and 2A. FEBS Lett. 1993:330(3):283-286. https://doi.org/10.1016/0014-5793(93)80889-3
Google Scholar: Author Only Title Only Author and Title

Jaakola L. New insights into the regulation of anthocyanin biosynthesis in fruits. Trends Plant Sci. 2013:18(9):477-483. https://doi.org/10.1016/j.tplants.2013.06.003
Google Scholar: Author Only Title Only Author and Title

Jalmi SK, Sinha AK. ROS mediated MAPK signaling in abiotic and biotic stress- striking similarities and differences. Front Plant Sci. 2015:6:769. https://doi.org/10.3389/fpls.2015.00769
Google Scholar: Author Only Title Only Author and Title

Janssens V, Goris J. Protein phosphatase 2A: a highly regulated family of serine/threonine phosphatases implicated in cell growth and signalling. Biochem J. 2001:353(3):417-439. https://doi.org/10.1042/0264-6021:3530417
Google Scholar: Author Only Title Only Author and Title

Jia M, Li X, Wang W, Li T, Dai Z, Chen Y, Zhang K, Zhu H, Mao W, Feng Q, et al. SnRK2 subfamily I protein kinases regulate ethylene biosynthesis by phosphorylating HB transcription factors to induce ACO1 expression in apple. New Phytol. 2022:234(4):1262-1277. https://doi.org/10.1111/nph.18040
Google Scholar: Author Only Title Only Author and Title

Jiang T, He Y, Wu Z, Cui Y, Wang X, Huang H, Fan Y, Han M, Wang J, Wang S, et al. Enhancing stimulation of cyaniding, GhLDOX3 activates reactive oxygen species to regulate tolerance of alkalinity negatively in cotton. Ecotox Environ Safe. 2023:267:115655. https://doi.org/10.1016/j.ecoenv.2023.115655
Google Scholar: Author Only Title Only Author and Title

Kamibayashi C, Lickteig RL, Estes R, Walter G, Mumby MC. Expression of the A subunit of protein phosphatase 2A and characterization of its interactions with the catalytic and regulatory subunits. J Biol Chem. 1992:267(30):21864-21872. https://doi.org/10.1016/s0021-9258(19)36692-x
Google Scholar: Author Only Title Only Author and Title

Kerchev P, Waszczak C, Lewandowska A, Willems P, Shapiguzov A, Li Z, Alseekh S, Muhlenbock P, Hoeberichts FA, Huang J, et al. Lack of GLYCOLATE OXIDASE1, but Not GLYCOLATE OXIDASE2, Attenuates the Photorespiratory Phenotype of CATALASE2-Deficient Arabidopsis. Plant Physiol. 2016:171(3):1704-1719. https://doi.org/10.1104/pp.16.00359
Google Scholar: Author Only Title Only Author and Title

Koes R, Verweij W, Quattrocchio F. Flavonoids: a colorful model for the regulation and evolution of biochemical pathways. Trends Plant Sci. 2005:10(5):236-242. https://doi.org/10.1016/j.tplants.2005.03.002
Google Scholar: Author Only Title Only Author and Title

Kovtun Y, Chiu WL, Tena G, Sheen J. Functional analysis of oxidative stress-activated mitogen-activated protein kinase cascade in plants. Proc Natl Acad Sci U S A. 2000:97(6):2940-2945. https://doi.org/10.1073/pnas.97.6.2940
Google Scholar: Author Only Title Only Author and Title

Landi M, Tattini M, Gould KS. Multiple functional roles of anthocyanins in plant-environment interactions. Environ Exp Bot. 2015:119:4-17. https://doi.org/10.1016/j.envexpbot.2015.05.012
Google Scholar: Author Only Title Only Author and Title

Lee DW, Gould KS. Why leaves turn red: pigments called anthocyanins probably protect leaves from light damage by direct shielding and by scavenging free radicals. AM SCI. 2002:90(6):524-531. https://doi.org/10.1511/2002.6.524
Google Scholar: Author Only Title Only Author and Title

Lesk C, Rowhani P, Ramankutty N. Influence of extreme weather disasters on global crop production. Nature. 2016:529(7584):84-87. https://doi.org/10.1038/nature16467
Google Scholar: Author Only Title Only Author and Title

Li Y, Wang Y, Tan S, Li Z, Yuan Z, Glanc M, Domjan D, Wang K, Xuan W, Guo Y, et al. Root Growth Adaptation is Mediated by PYLs ABA Receptor-PP2A Protein Phosphatase Complex. Adv Sci. 2020:7(3):1901455. https://doi.org/10.1002/advs.201901455
Google Scholar: Author Only Title Only Author and Title

Li YY, Mao K, Zhao C, Zhao XY, Zhang HL, Shu HR, Hao YJ. MdCOP1 ubiquitin E3 ligases interact with MdMYB1 to regulate light-induced anthocyanin biosynthesis and red fruit coloration in apple. Plant Physiol. 2012:160(2):1011-1022. https://doi.org/10.1104/pp.112.199703
Google Scholar: Author Only Title Only Author and Title

Lillo C, Kataya AR, Heidari B, Creighton MT, Nemie-Feyissa D, Ginbot Z, Jonassen EM. Protein phosphatases PP2A, PP4 and PP6: mediators and regulators in development and responses to environmental cues. Plant Cell Environ. 2014:37(12):2631-2648. https://doi.org/10.1111/pce.12364
Google Scholar: Author Only Title Only Author and Title

Lin-Wang K, Micheletti D, Palmer J, Volz R, Lozano L, Espley R, Hellens RP, Chagne D, Rowan DD, Troggio M, et al. High temperature reduces apple fruit colour via modulation of the anthocyanin regulatory complex. Plant Cell Environ. 2011:34(7):1176-1190. https://doi.org/10.1111/j.1365-3040.2011.02316.x
Google Scholar: Author Only Title Only Author and Title

Livak KJ, Schmittgen TD. Analysis of relative gene expression data using real-time quantitative PCR and the 2-△△CT method. Methods. 2001:25(4):402-408. https://doi.org/10.1006/meth.2001.1262
Google Scholar: Author Only Title Only Author and Title

Mine A, Berens ML, Nobori T, Anver S, Fukumoto K, Winkelmuller TM, Takeda A, Becker D, Tsuda K. Pathogen exploitation of an abscisic acid- and jasmonate-inducible MAPK phosphatase and its interception by Arabidopsis immunity. Proc Natl Acad Sci U S A. 2017:114(28):7456-7461. https://doi.org/10.1073/pnas.1702613114
Google Scholar: Author Only Title Only Author and Title

Mittler R. ROS Are Good. Trends Plant Sci. 2017:22(1):11-19. https://doi.org/10.1016/j.tplants.2016.08.002
Google Scholar: Author Only Title Only Author and Title

Mittler R, Zandalinas SI, Fichman Y, Van Breusegem F. Reactive oxygen species signalling in plant stress responses. Nat Rev Mol Cell Biol. 2022:23(10):663-679. https://doi.org/10.1038/s41580-022-00499-2
Google Scholar: Author Only Title Only Author and Title

Nakabayashi R, Yonekura-Sakakibara K, Urano K, Suzuki M, Yamada Y, Nishizawa T, Matsuda F, Kojima M, Sakakibara H, Shinozaki K, et al. Enhancement of oxidative and drought tolerance in Arabidopsis by overaccumulation of antioxidant flavonoids. Plant J. 2014:77(3):367-379. https://doi.org/10.1111/tpj.12388
Google Scholar: Author Only Title Only Author and Title

Neill SO, Gould KS, Kilmartin PA, Mitchell KA, Markham KR. Antioxidant activities of red versus green leaves in Elatostema rugosum. Plant Cell Environ. 2002:25(4):539-547. https://doi.org/10.1046/j.1365-3040.2002.00837.x
Google Scholar: Author Only Title Only Author and Title

Ni J, Wang S, Yu W, Liao Y, Pan C, Zhang M, Tao R, Wei J, Gao Y, Wang D, et al. The ethylene-responsive transcription factor PpERF9 represses PpRAP2.4 and PpMYB114 via histone deacetylation to inhibit anthocyanin biosynthesis in pear. Plant Cell. 2023:35(6):2271-2292. https://doi.org/10.1093/plcell/koad077
Google Scholar: Author Only Title Only Author and Title

Olsson AS, Engström P, Söderman E. The homeobox genes ATHB12 and ATHB7 encode potential regulators of growth in response to water deficit in Arabidopsis. Plant Mol Biol. 2004:55(5):663-677. https://doi.org/10.1007/s11103-004-1581-4
Google Scholar: Author Only Title Only Author and Title

Qu Y, Bai X, Zhu YJ, Qi R, Tian G, Wang Y, Li YH, Zhang KM. Reactive Oxygen Species Acts as an Important Inducer in Low-temperature-induced Anthocyanin Biosynthesis in Begonia semperflorens. J Am Soc Hortic Sci. 2018:143(6):486-493. https://doi.org/10.21273/JASHS04488-18
Google Scholar: Author Only Title Only Author and Title

Ren H, Rao J, Tang M, Li Y, Dang X, Lin D. PP2A interacts with KATANIN to promote microtubule organization and conical cell morphogenesis. J Integr Plant Biol. 2022:64(8):1514-1530. https://doi.org/10.1111/jipb.13281
Google Scholar: Author Only Title Only Author and Title

Ruediger R, Hentz M, Fait J, Mumby M, Walter G. Molecular model of the A subunit of protein phosphatase 2A interaction with other subunits and tumor antigens. J Virol. 1994:68(1):123-129. https://doi.org/10.1128/JVI.68.1.123-129.1994
Google Scholar: Author Only Title Only Author and Title

Schaart JG, Dubos C, De La Fuente IR, van Houwelingen AMML, de Vos RCH, Jonker HH, Xu WJ, Routaboul JM, Lepiniec L, Bovy AG. Identification and characterization of MYB-bHLH-WD40 regulatory complexes controlling proanthocyanidin biosynthesis in strawberry (Fragaria × ananassa) fruits. New Phytol. 2012:197(2):454-467. https://doi.org/10.1111/nph.12017
Google Scholar: Author Only Title Only Author and Title

Shan X, Zhang Y, Peng W, Wang Z, Xie D. Molecular mechanism for jasmonate-induction of anthocyanin accumulation in Arabidopsis. J Exp Bot. 2009:60(13):3849-3860. https://doi.org/10.1093/jxb/erp223
Google Scholar: Author Only Title Only Author and Title

Shi H, Liu G, Wei Y, Chan Z. The zinc-finger transcription factor ZAT6 is essential for hydrogen peroxide induction of anthocyanin synthesis in Arabidopsis. Plant Mol Biol. 2018:97(1-2):165-176. https://doi.org/10.1007/s11103-018-0730-0
Google Scholar: Author Only Title Only Author and Title

Soderman E, Mattsson J, Engstrom P. The Arabidopsis homeobox gene ATHB-7 is induced by water deficit and by abscisic acid. Plant J. 1996:10(2):375-381. https://doi.org/10.1046/j.1365-313x.1996.10020375.x
Google Scholar: Author Only Title Only Author and Title

Söderman E, Hjellström M, Fahleson J, Engström P. The HD-Zip gene ATHB6 in Arabidopsis is expressed in developing leaves, roots and carpels and up-regulated by water deficit conditions. Plant Mol Biol. 1999:40(6):1073-1083. https://doi.org/10.1023/A:1006267013170
Google Scholar: Author Only Title Only Author and Title

Steyn WJ, Wand SJE, Holcroft DM, Jacobs G. Anthocyanins in vegetative tissues: a proposed unified function in photoprotection. New Phytol. 2002:155(3):349-361. https://doi.org/10.1046/j.1469-8137.2002.00482.x
Google Scholar: Author Only Title Only Author and Title

Takos AM, Jaffe FW, Jacob SR, Bogs J, Robinson SP, Walker AR. Light-induced expression of a MYB gene regulates anthocyanin

biosynthesis in red apples. Plant Physiol. 2006:142(3):1216-1232. https://doi.org/10.1104/pp.106.088104
Google Scholar: Author Only Title Only Author and Title

Uhrig RG, Labandera AM, Moorhead GB. Arabidopsis PPP family of serine/threonine protein phosphatases: many targets but few engines. Trends Plant Sci. 2013:18(9):505-513. https://doi.org/10.1016/j.tplants.2013.05.004
Google Scholar: Author Only Title Only Author and Title

Wang L, Leister D, Guan L, Zheng Y, Schneider K, Lehmann M, Apel K, Kleine T. The Arabidopsis SAFEGUARD1 suppresses singlet oxygen-induced stress responses by protecting grana margins. Proc Natl Acad Sci U S A. 2020:117(12):6918-6927. https://doi.org/10.1073/pnas.1918640117
Google Scholar: Author Only Title Only Author and Title

Winkel-Shirley B. Flavonoid biosynthesis. A colorful model for genetics, biochemistry, cell biology, and biotechnology. Plant Physiol. 2001:126(2):485-493. https://doi.org/10.1104/pp.126.2.485
Google Scholar: Author Only Title Only Author and Title

Xie XB, Li S, Zhang RF, Zhao J, Chen YC, Zhao Q, Yao YX, You CX, Zhang XS, Hao YJ. The bHLH transcription factor MdbHLH3 promotes anthocyanin accumulation and fruit colouration in response to low temperature in apples. Plant Cell Environ. 2012:35(11):1884-1897. https://doi.org/10.1111/j.1365-3040.2012.02523.x
Google Scholar: Author Only Title Only Author and Title

Xu H, Zou Q, Yang G, Jiang S, Fang H, Wang Y, Zhang J, Zhang Z, Wang N, Chen X. MdMYB6 regulates anthocyanin formation in apple both through direct inhibition of the biosynthesis pathway and through substrate removal. Hortic Res. 2020:7(1):72. https://doi.org/10.1038/s41438-020-0294-4
Google Scholar: Author Only Title Only Author and Title

Xu W, Dubos C, Lepiniec L. Transcriptional control of flavonoid biosynthesis by MYB-bHLH-WDR complexes. Trends Plant Sci. 2015:20(3):176-185. https://doi.org/10.1016/j.tplants.2014.12.001
Google Scholar: Author Only Title Only Author and Title

Xu Z, Mahmood K, Rothstein SJ. ROS Induces Anthocyanin Production Via Late Biosynthetic Genes and Anthocyanin Deficiency Confers the Hypersensitivity to ROS-Generating Stresses in Arabidopsis. Plant Cell Physiol. 2017:58(8):1364-1377. https://doi.org/10.1093/pcp/pcx073
Google Scholar: Author Only Title Only Author and Title

Zhang D, Yu B, Bai J, Qian M, Shu Q, Su J, Teng Y. Effects of high temperatures on UV-B/visible irradiation induced postharvest anthocyanin accumulation in 'Yunhongli No. 1' (Pyrus pyrifolia Nakai) pears. Sci Hortic. 2012:134:53-59. https://doi.org/10.1016/j.scienta.2011.10.025
Google Scholar: Author Only Title Only Author and Title

Zhang L, Tao R, Wang S, Gao Y, Wang L, Yang S, Zhang X, Yu W, Wu X, Li K, et al. PpZAT5 suppresses the expression of a B-box gene PpBBX18 to inhibit anthocyanin biosynthesis in the fruit peel of red pear. Front Plant Sci. 2022:13:1022034. https://doi.org/10.3389/fpls.2022.1022034
Google Scholar: Author Only Title Only Author and Title

Zhou HW, Nussbaumer C, Chao Y, DeLong A. Disparate roles for the regulatory A subunit isoforms in Arabidopsis protein phosphatase 2A. Plant Cell. 2004:16(3):709-722. https://doi.org/10.1105/tpc.018994
Google Scholar: Author Only Title Only Author and Title